Understanding the effects of stellar FEEDBACK in RCW49: Observations and models

Maitraiyee Tiwari (UMD)

M. Pound, M. Wolfire, R. Karim, E. Tarantino,
X. Tielens, N. Schneider and the FEEDBACK consortium

RCW 49

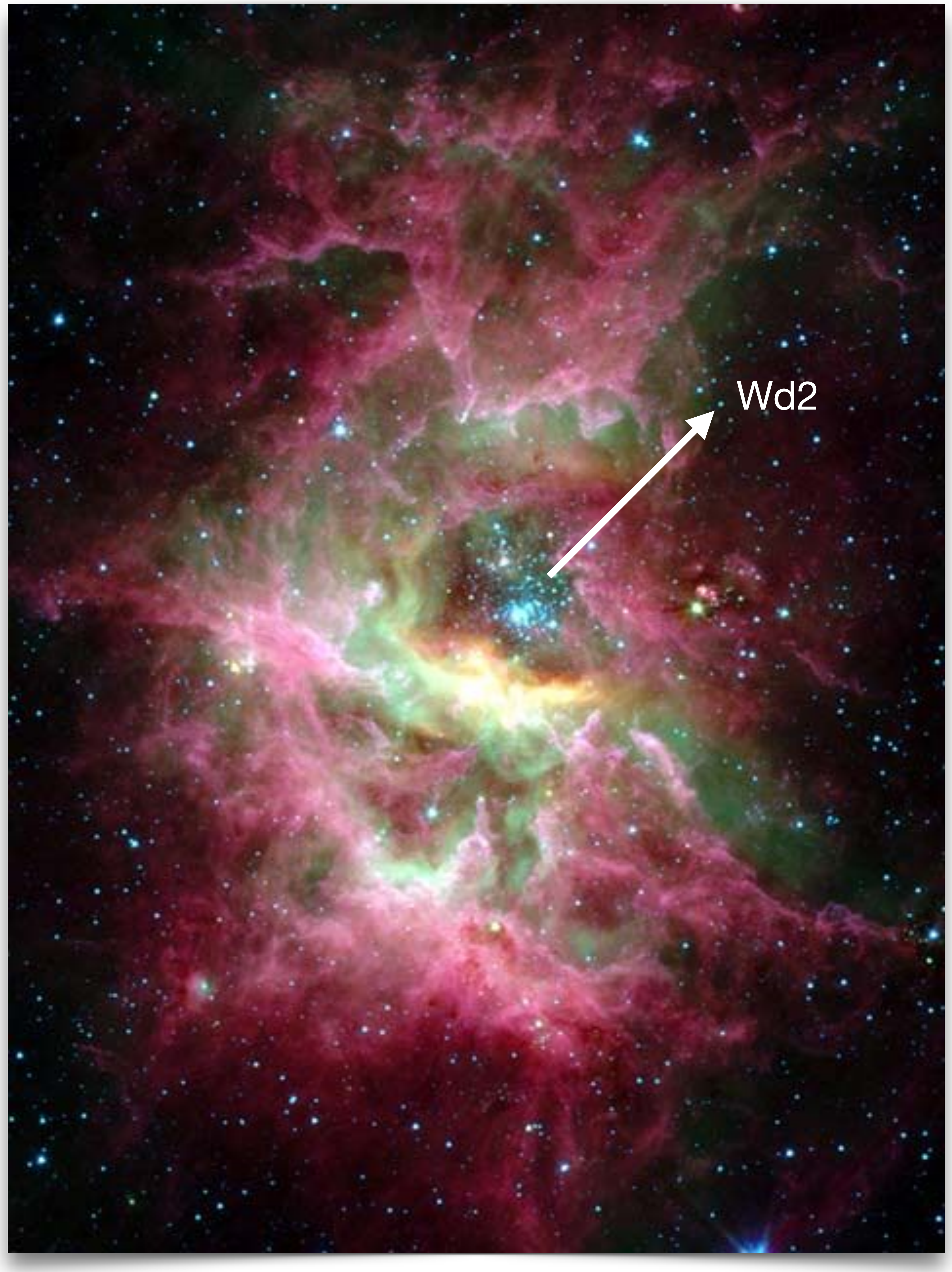

One of the most luminous massive star-forming regions in our Galaxy!

- It is 4.16 kpc away from us.
- It has a compact stellar cluster Wd2: 37 OB stars and 30 early type OB star candidates.
- It has 2 Wolf Rayet stars + O5V star east of Wd2.

RCW 49

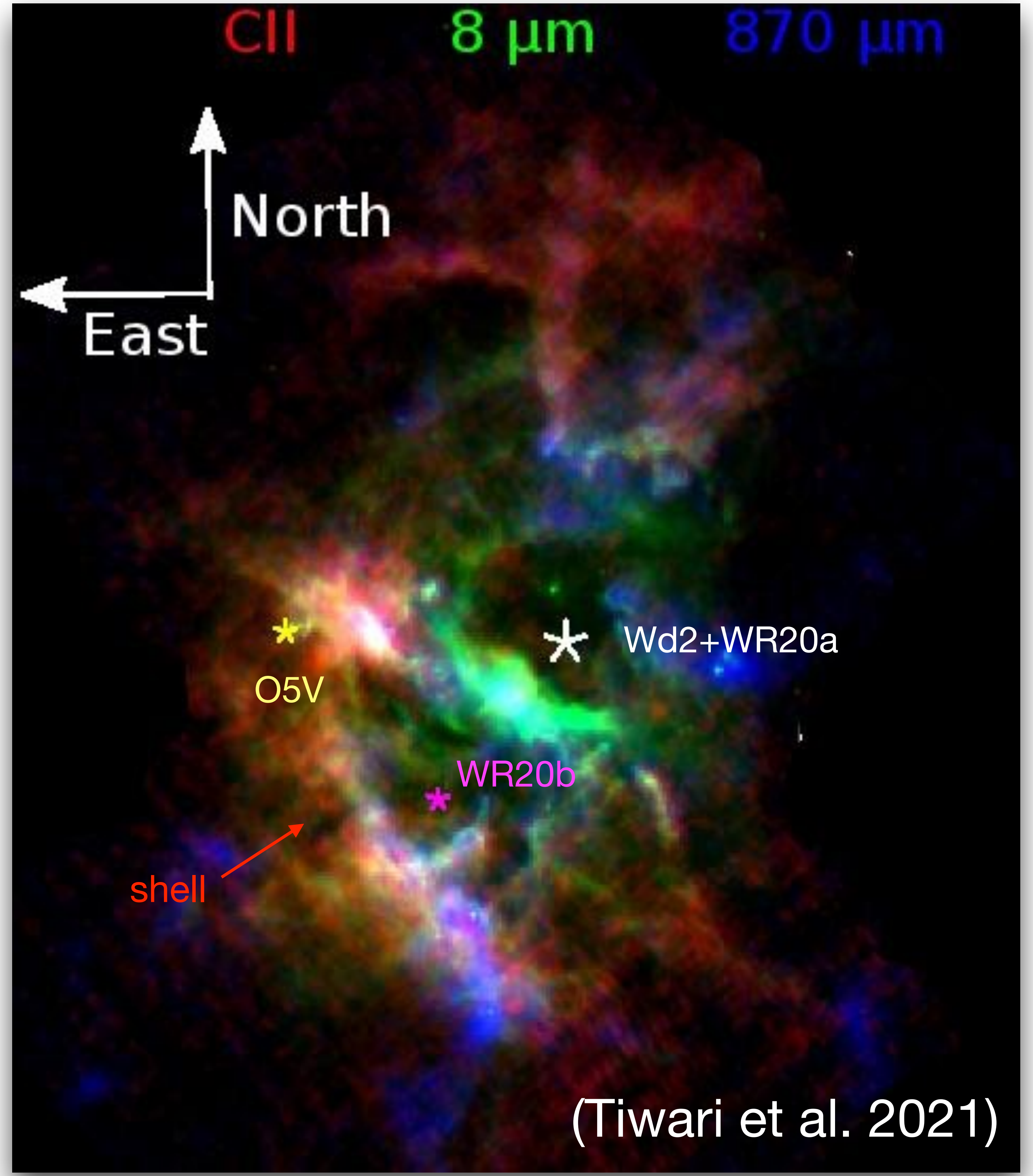

Multi-wavelength overview of different gas components:

- CII emission traces the warm PDR shell
- 8μm emission traces the warm dust
- 870 μm emission traces the cold and dense clumps

New FEEDBACK observations

CO (3-2) observations

CII (158μm) and OI (63μm) observations

Average spectra

A complex set of gas components

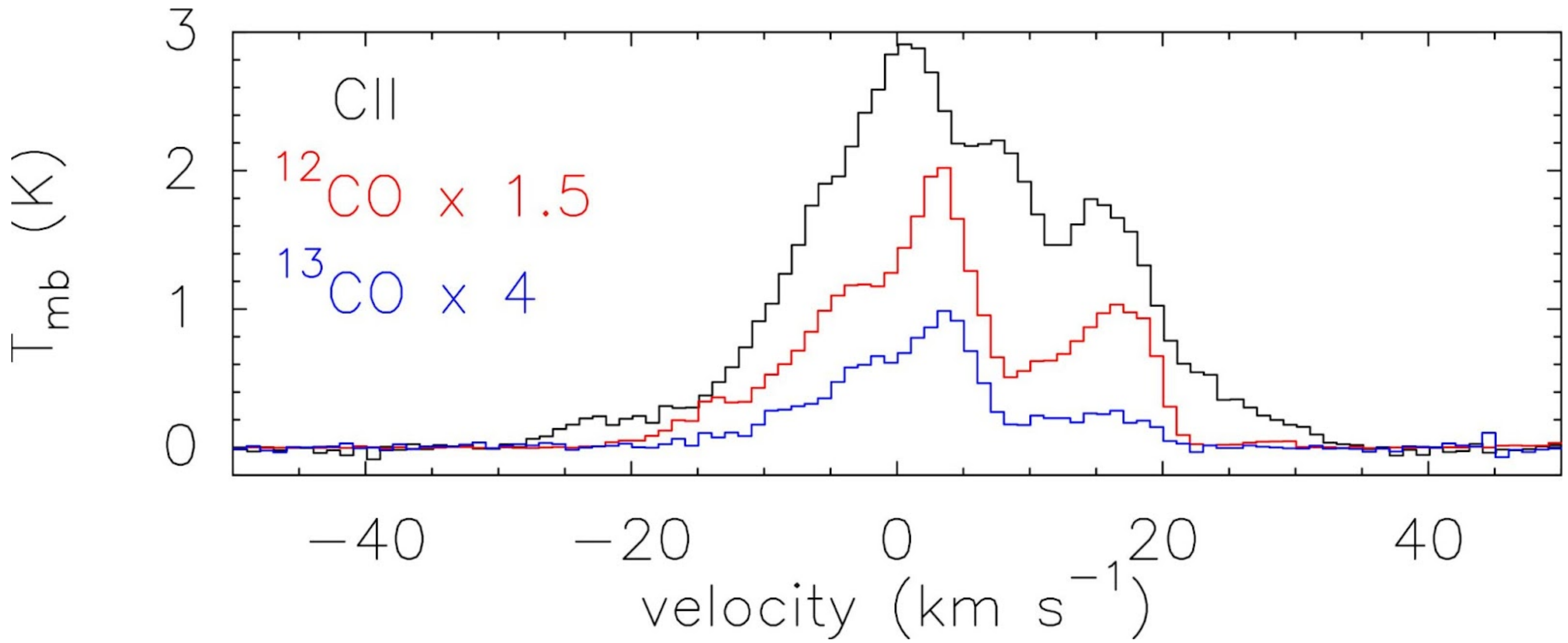

(Tiwari et al. 2021)

Emission maps

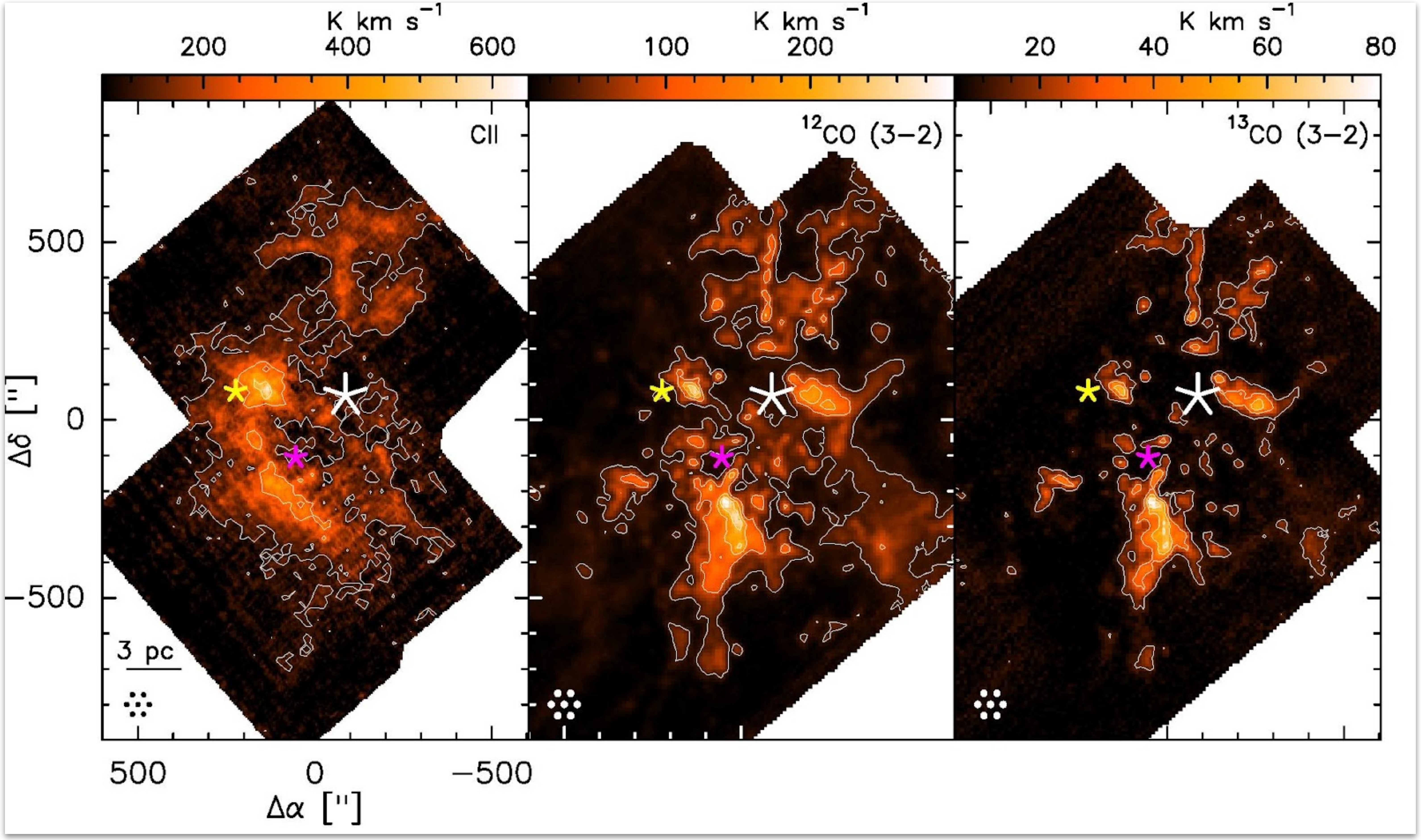

Maps in the entire velocity range.

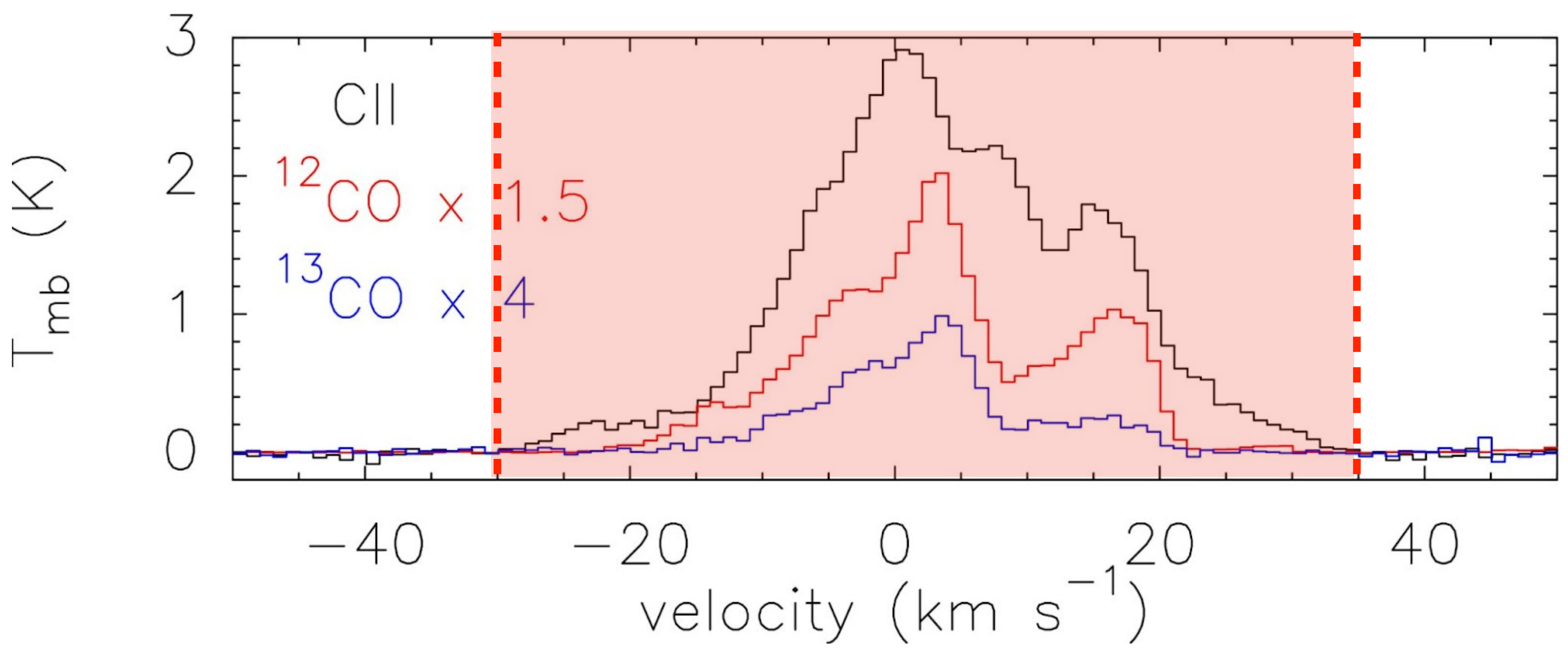

(Tiwari et al. 2021)

Disentangling different structures

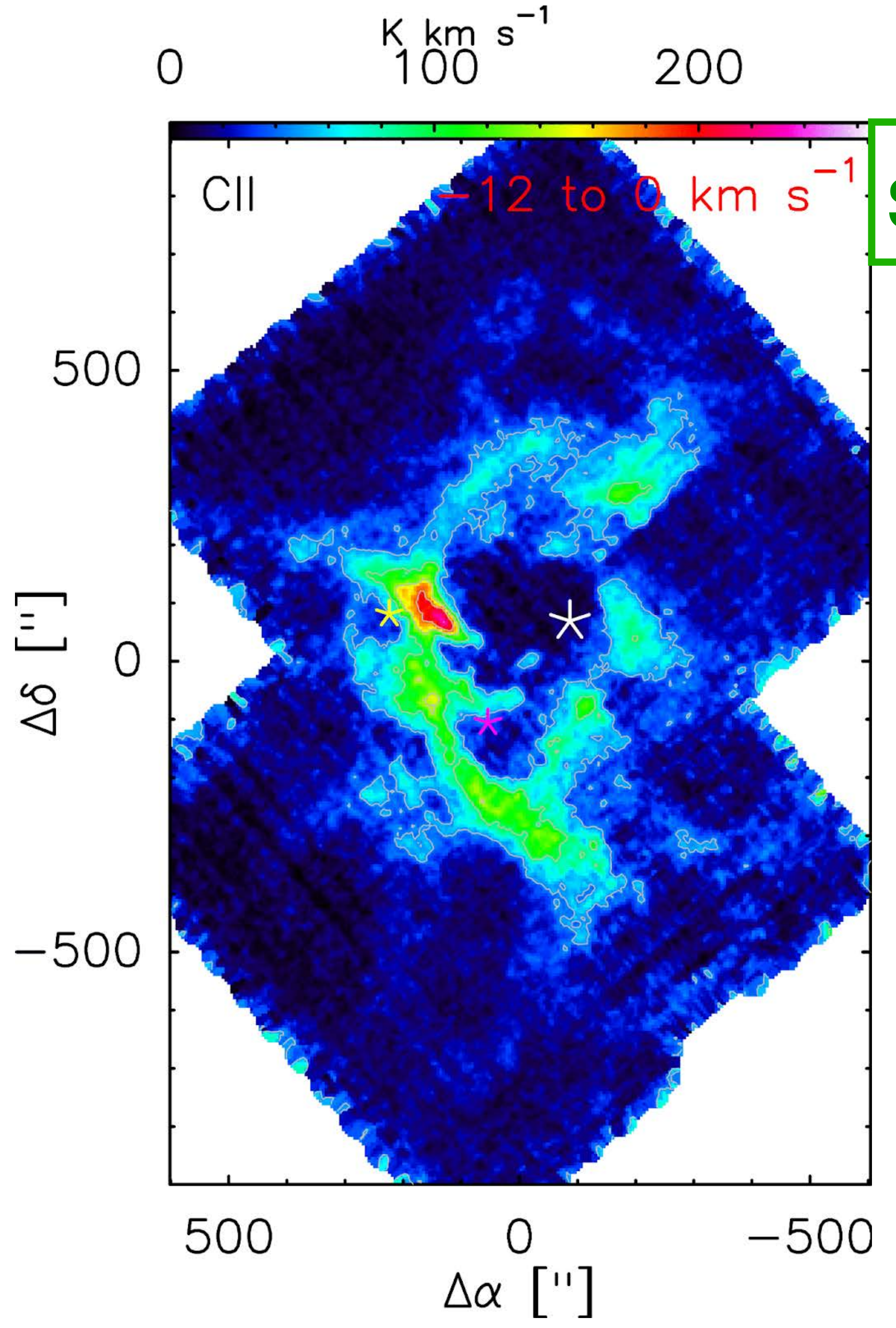

shell

Average spectra for the map

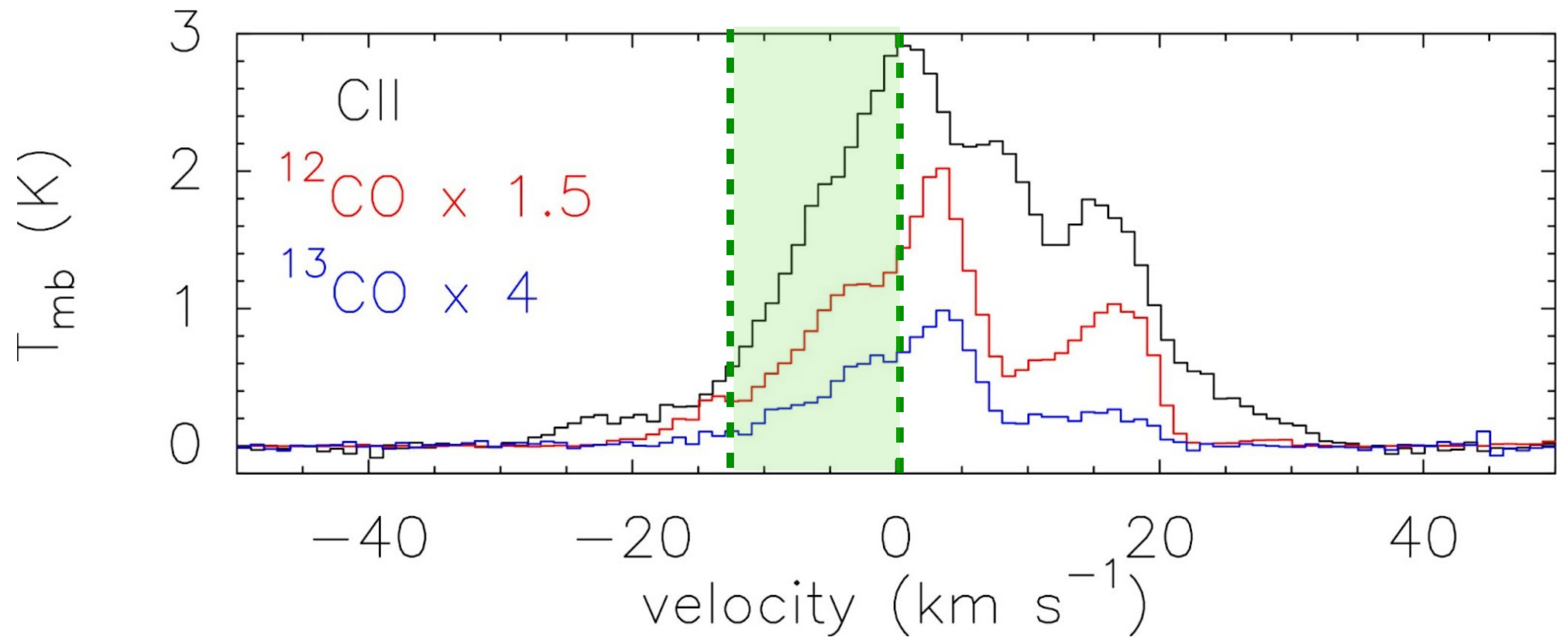

(Tiwari et al., to be sub.)

Disentangling different structures

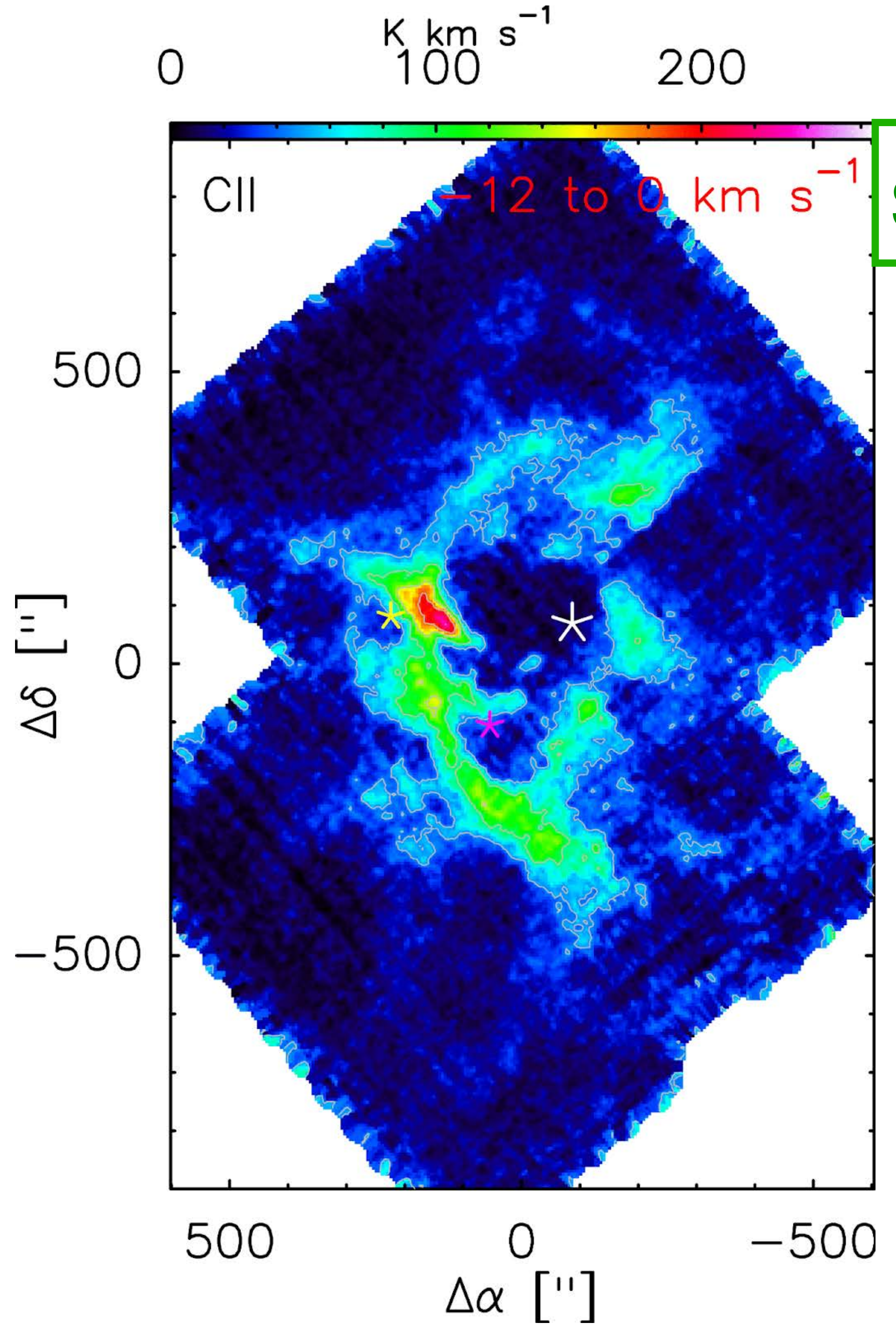

shell

Average spectra for the map

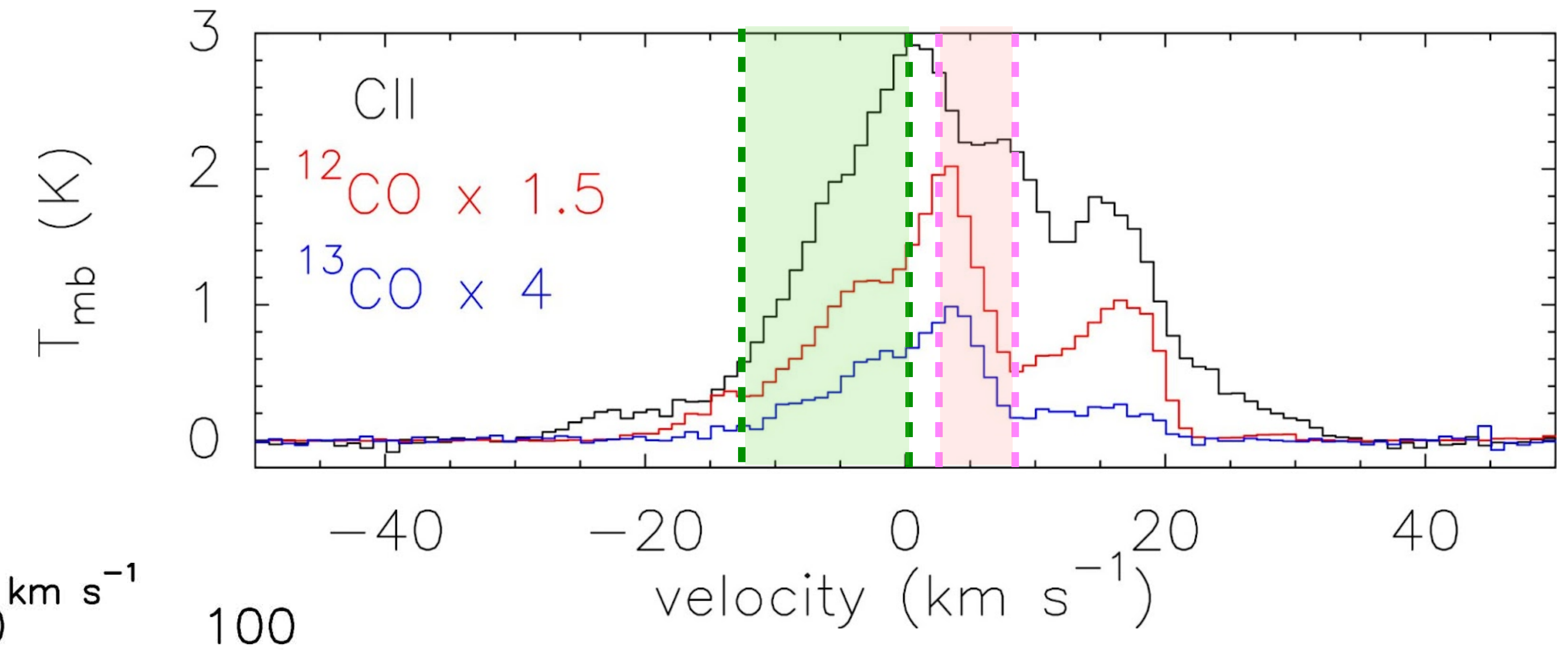

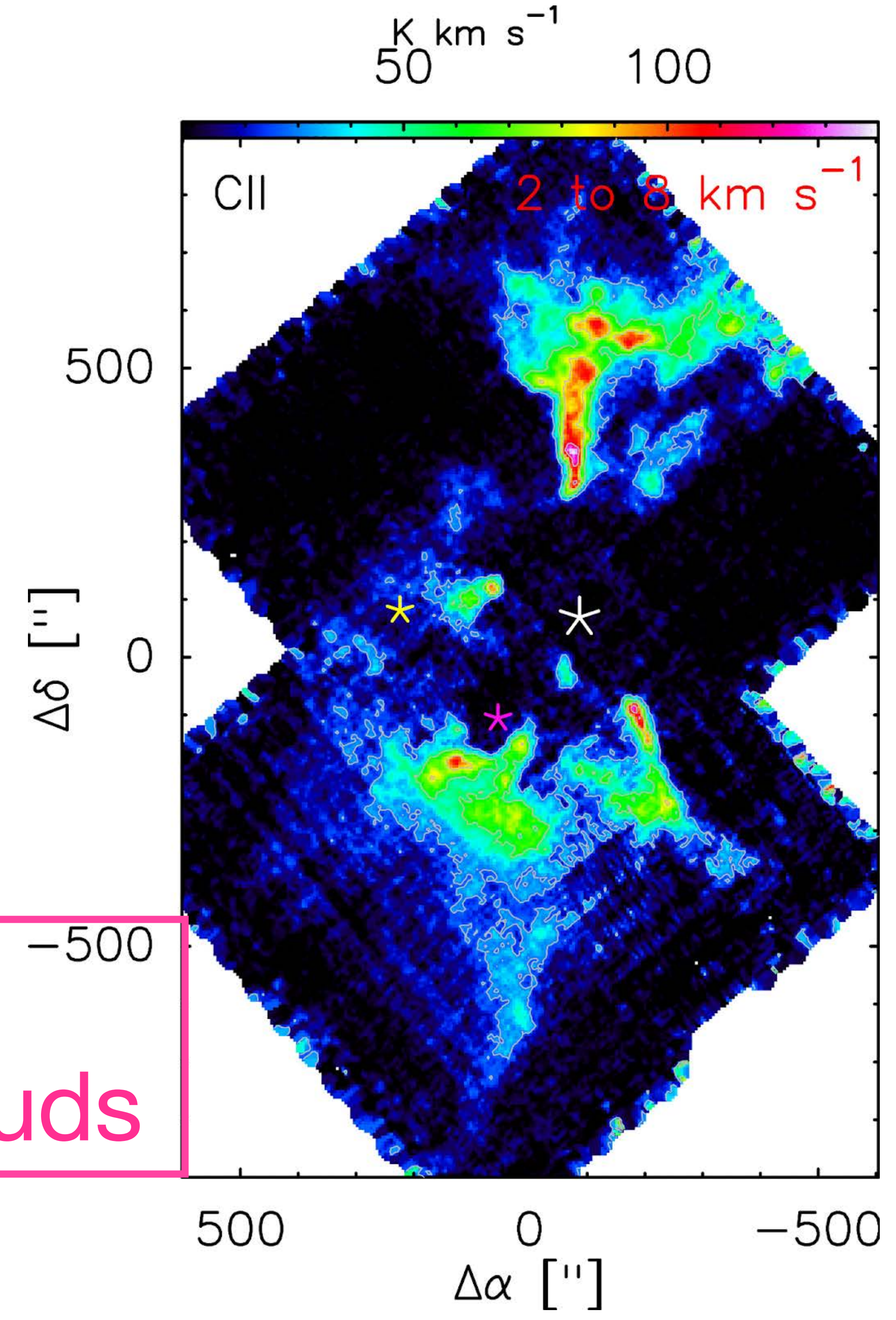

northern &
southern clouds

(Tiwari et al., to be sub.)

Disentangling different structures

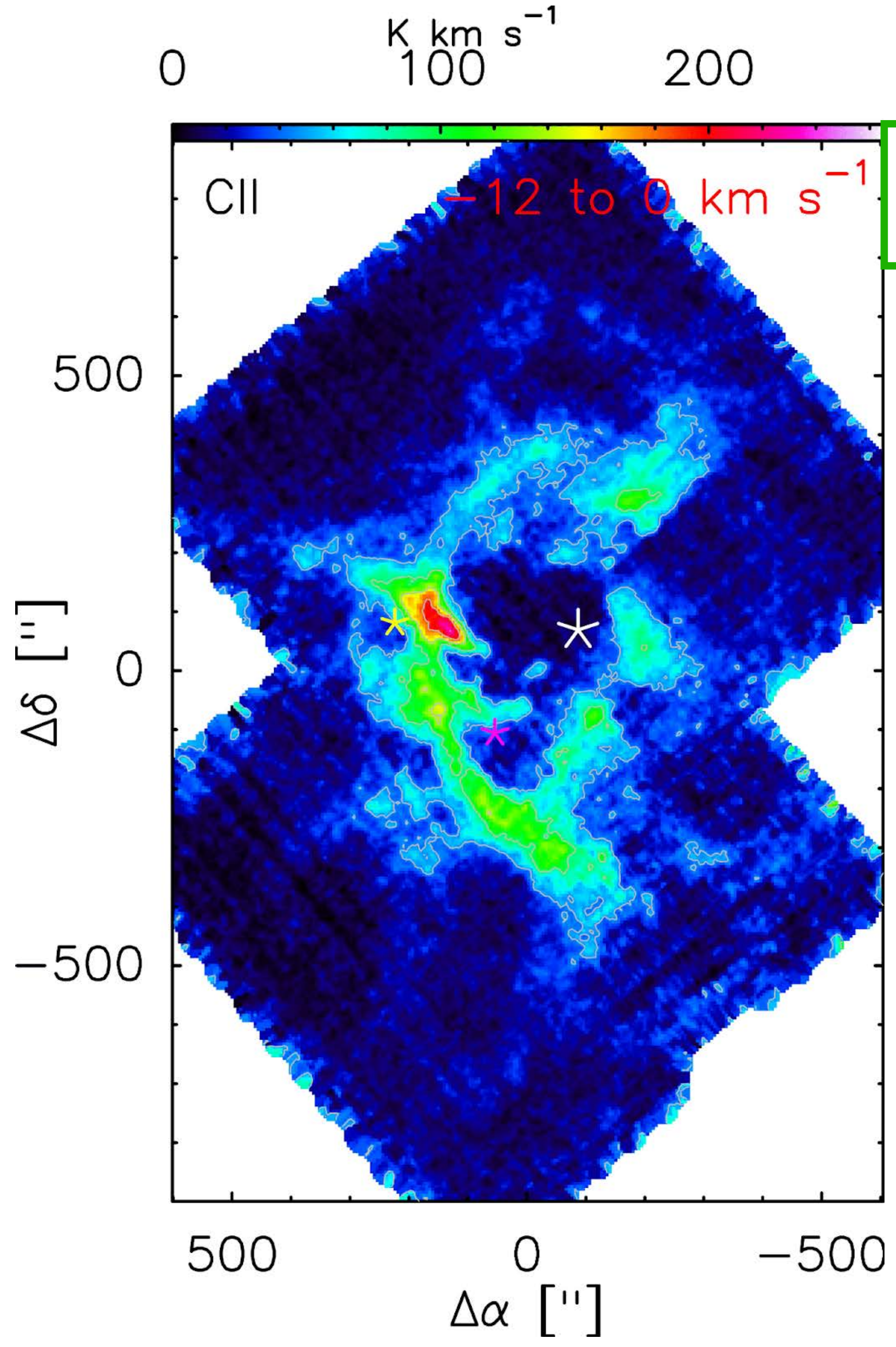

shell

Average spectra for the map

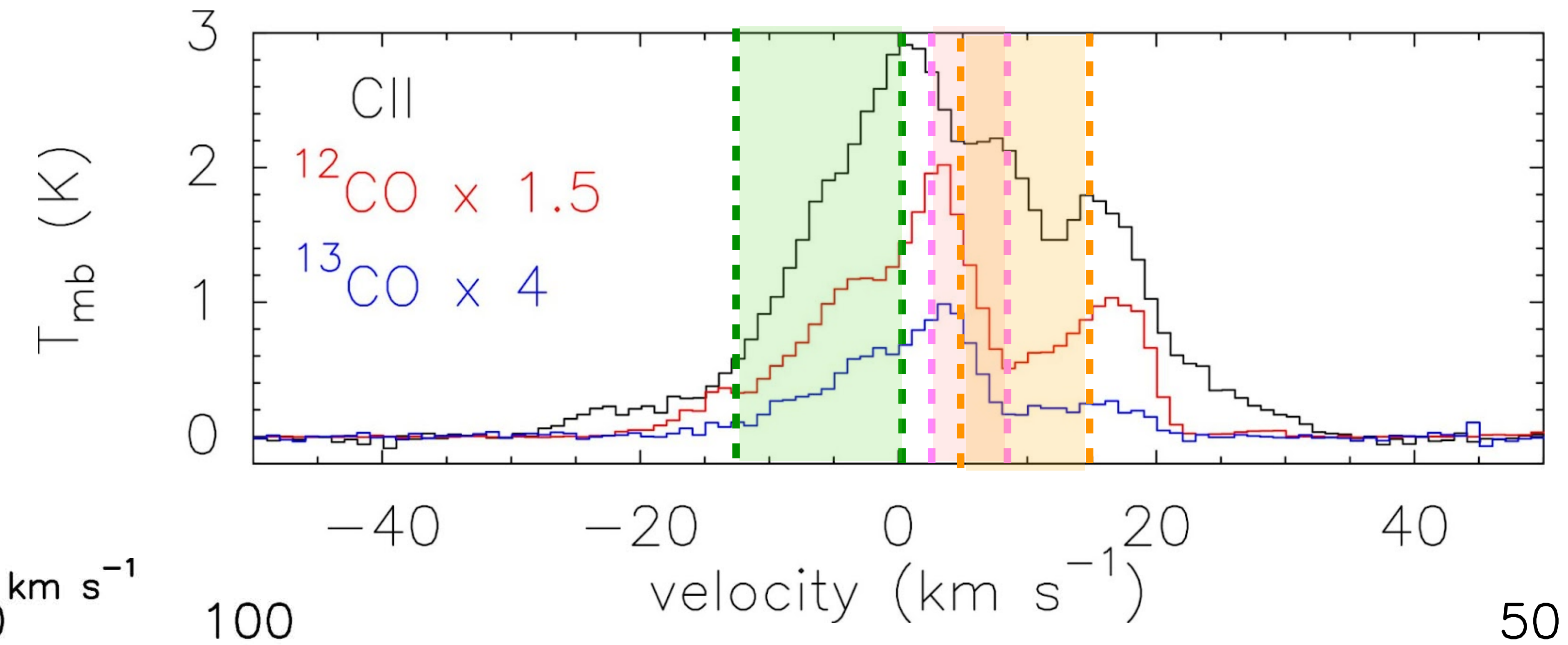

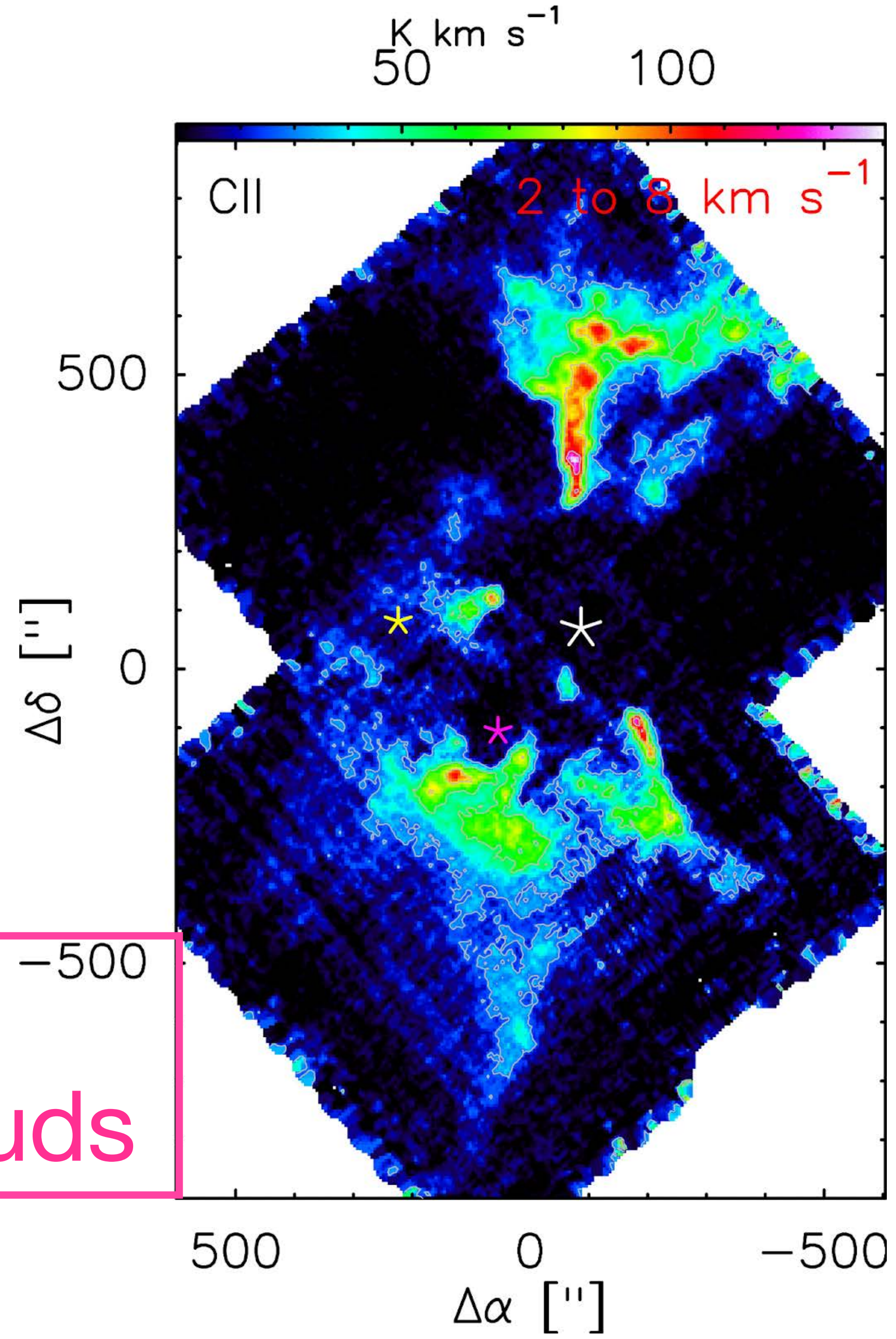

northern & southern clouds

pillar

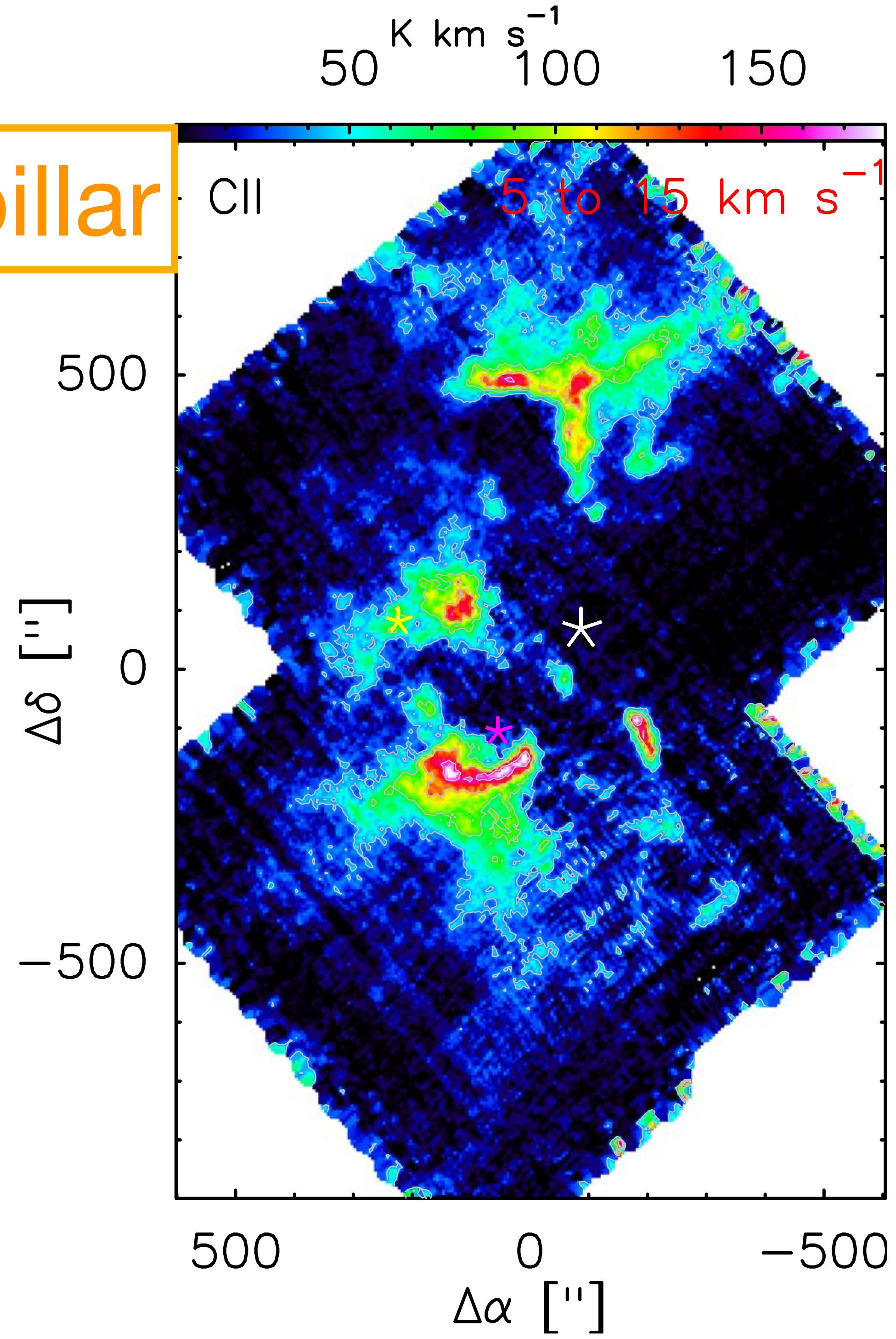

(Tiwari et al., to be sub.)

Disentangling different structures

Average spectra for the map

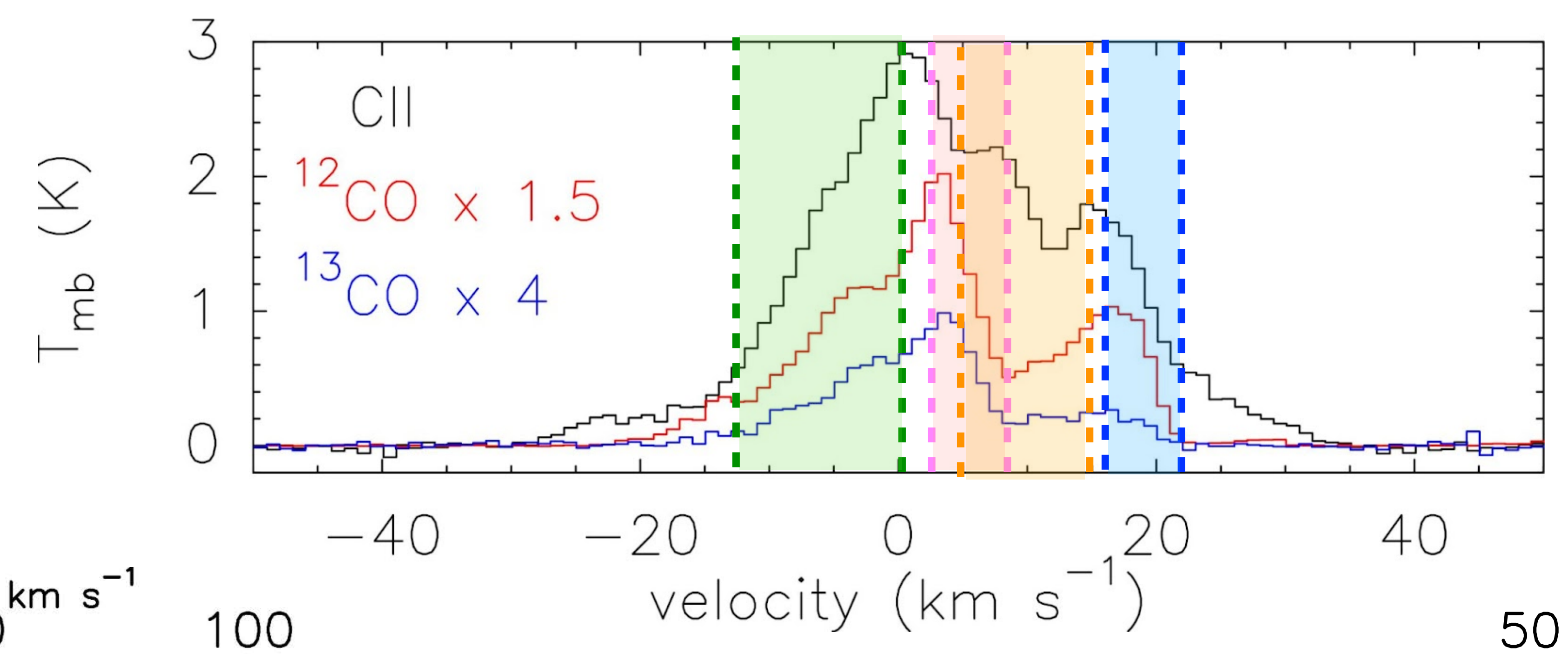

shell

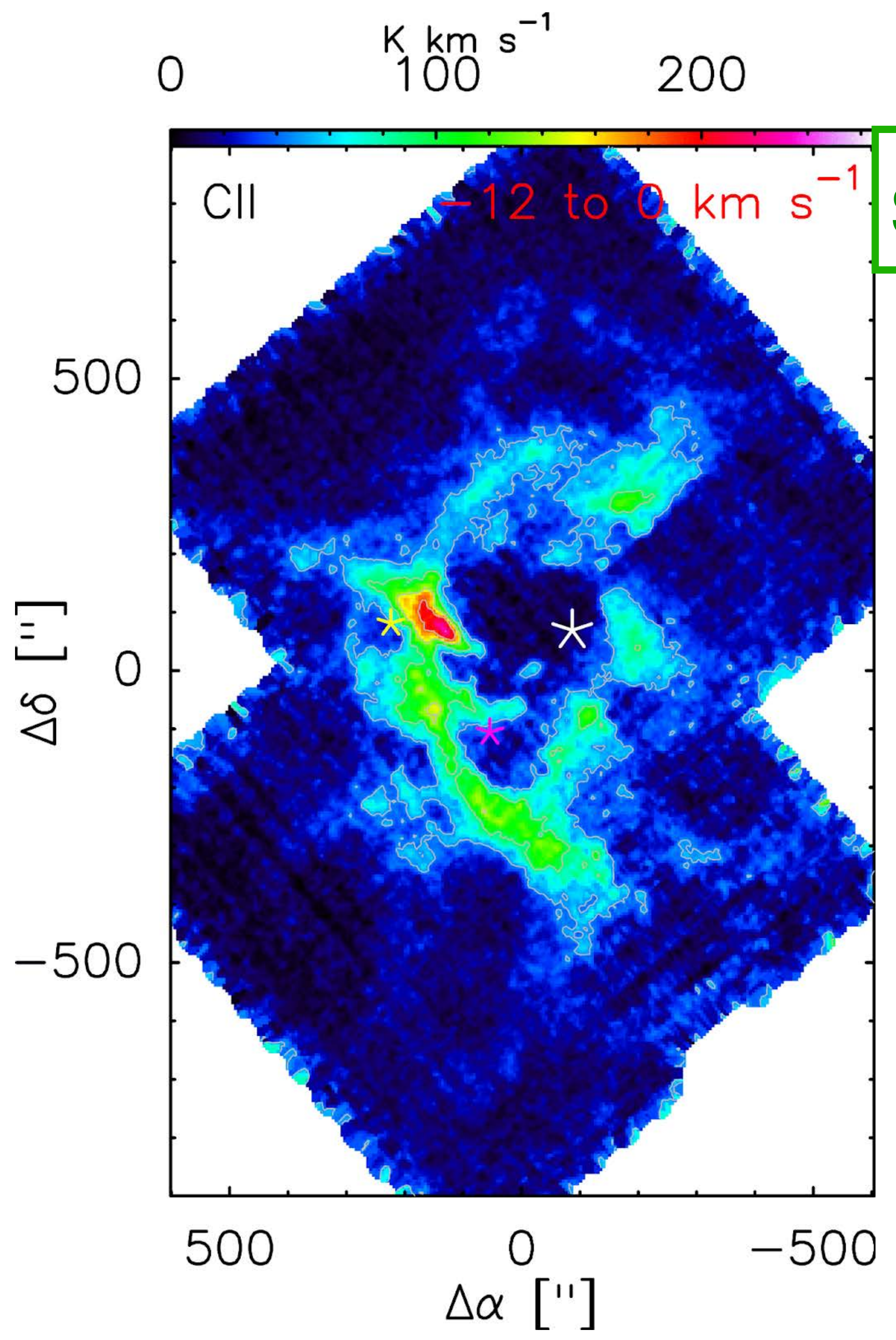

ridge

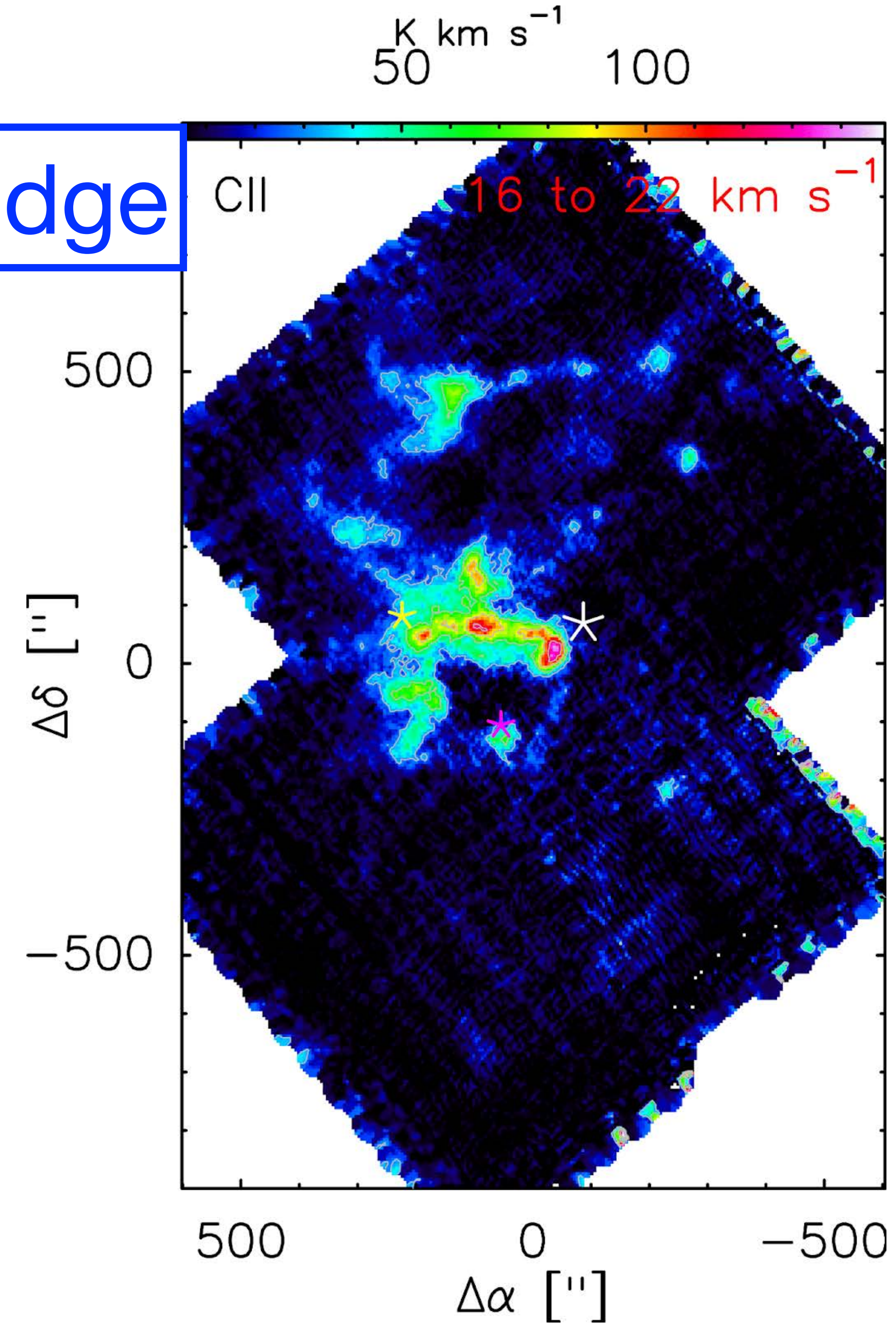

northern &
southern clouds

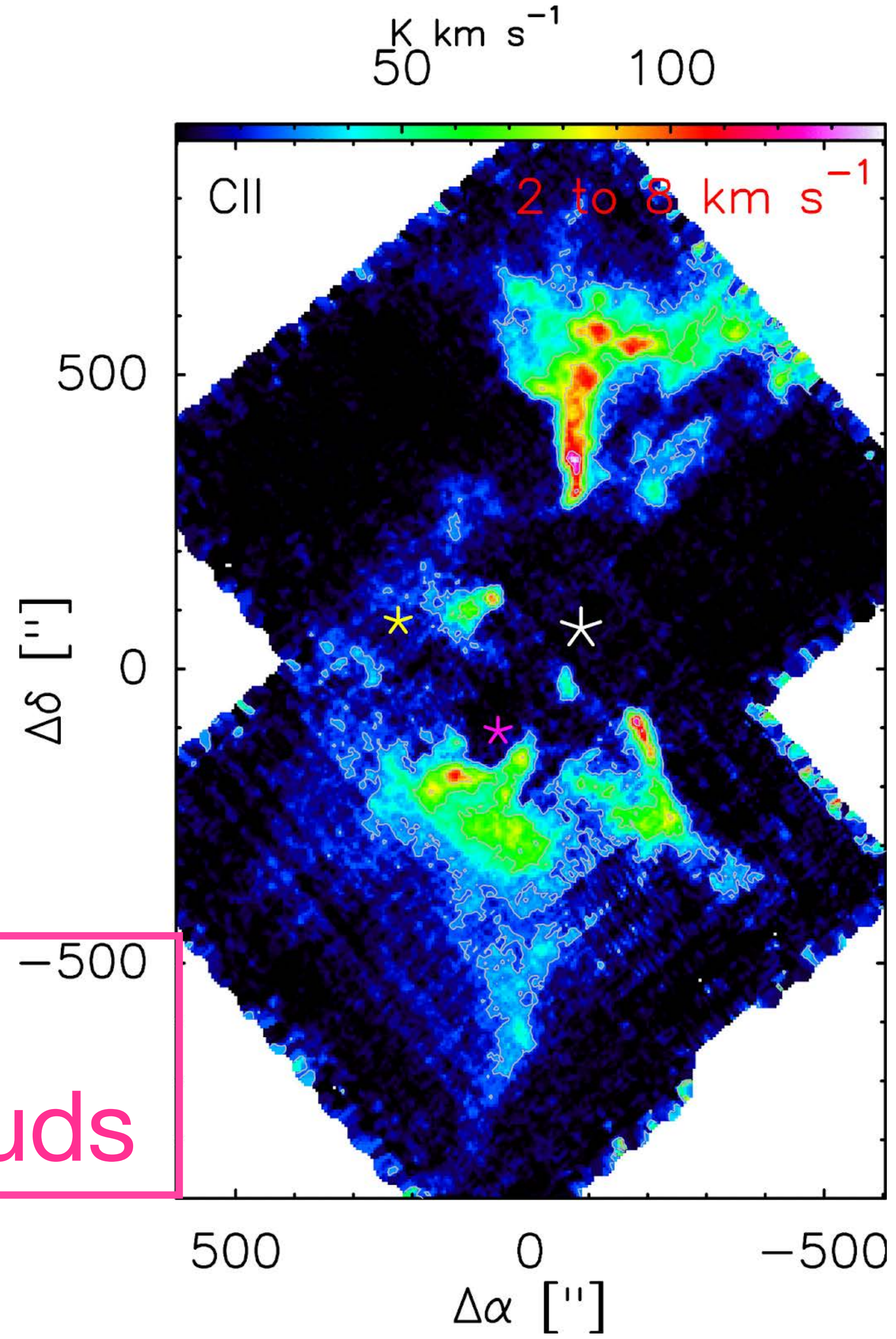

pillar

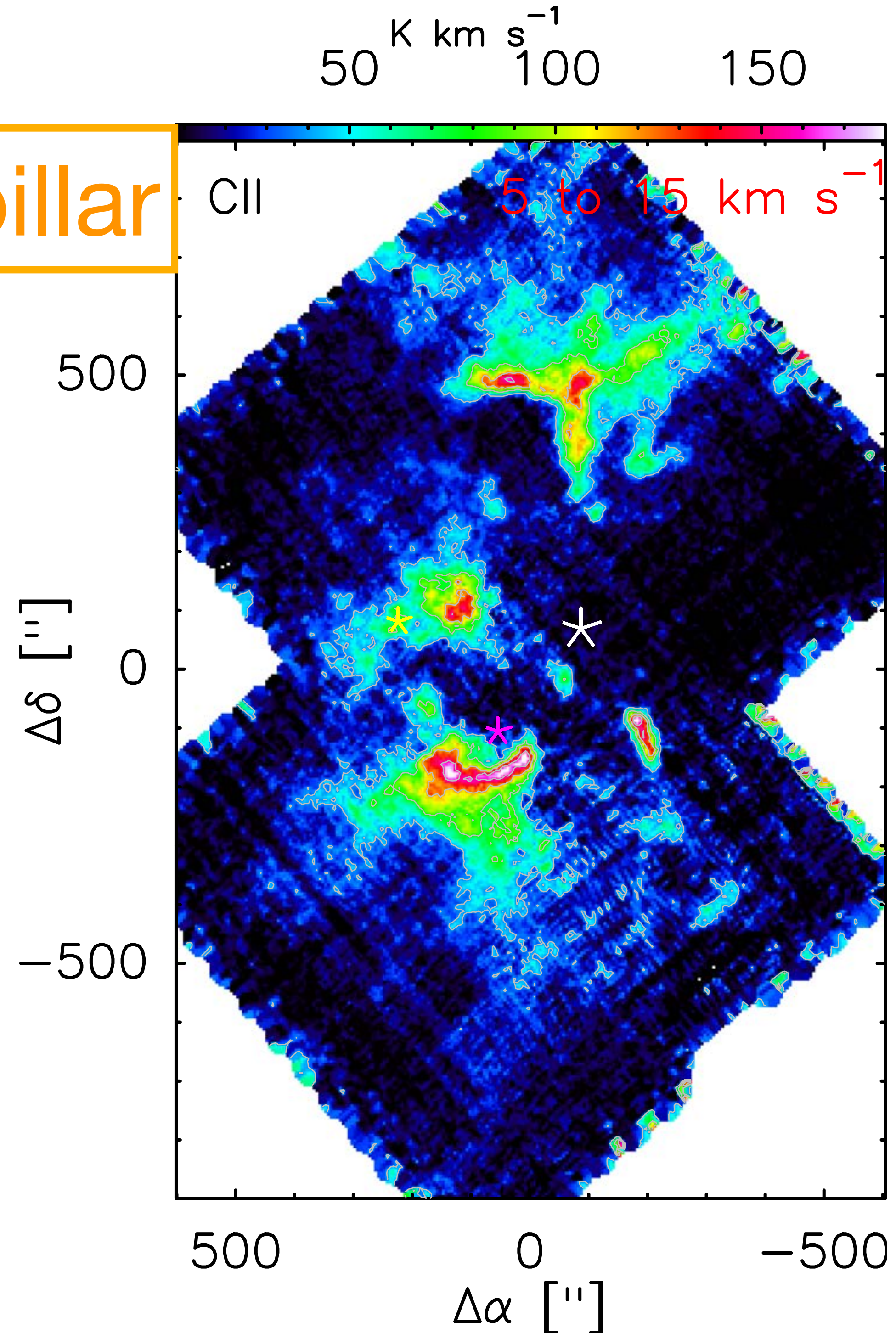

(Tiwari et al., to be sub.)

Interesting regions in RCW 49

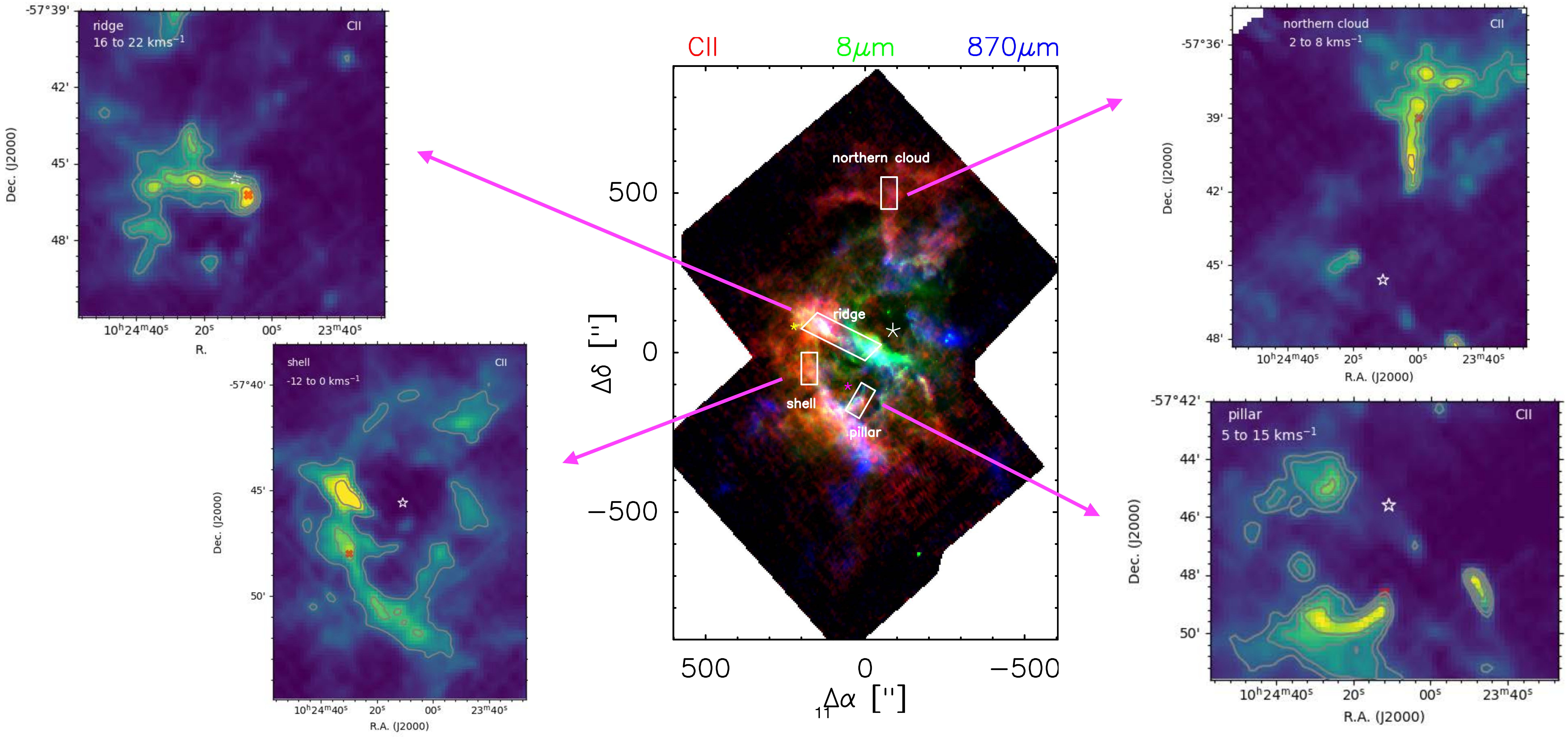

Previous studies: shell

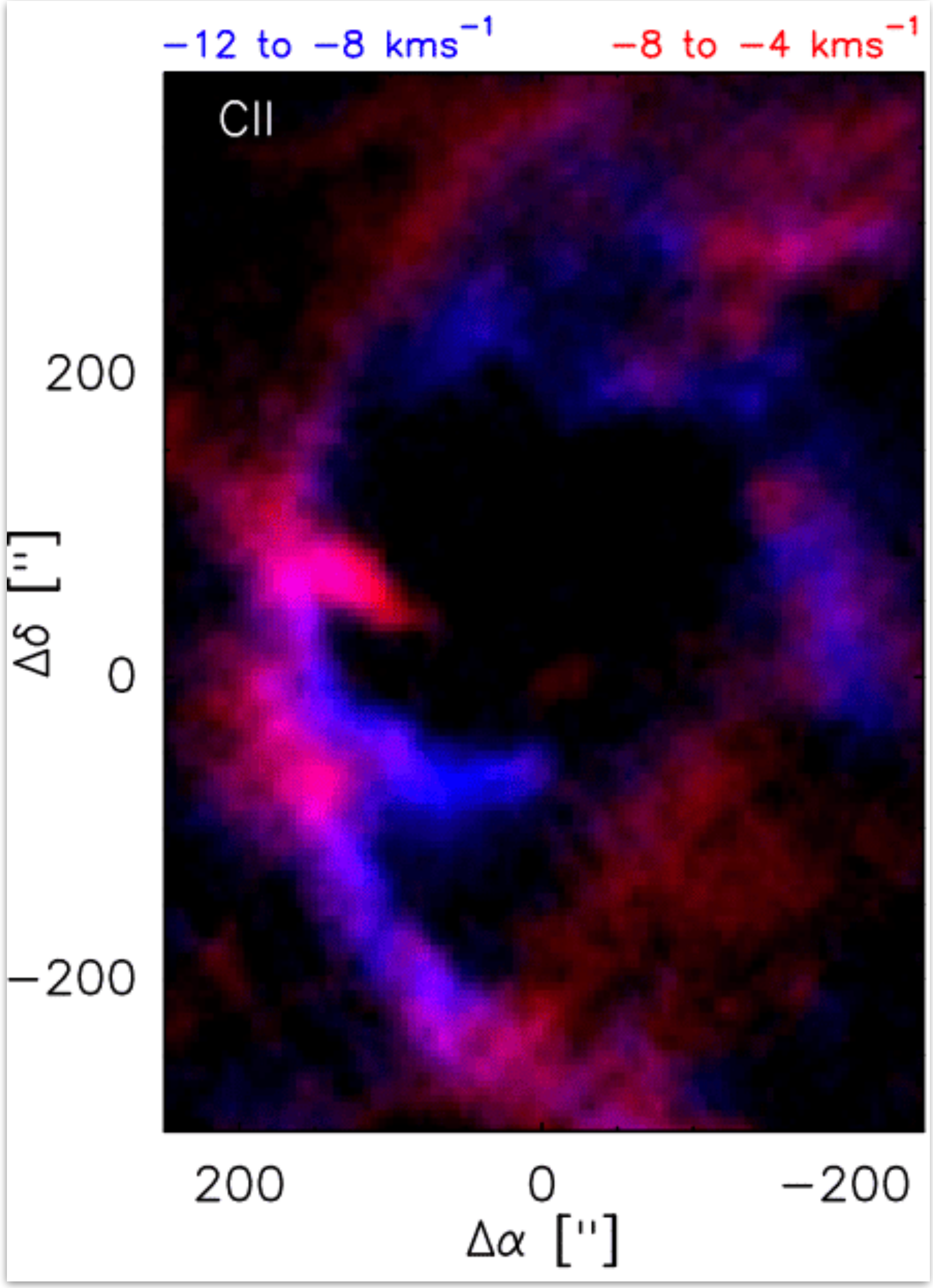

The expanding shell of RCW 49 (Tiwari et al., 2021)

Shell parameters:

- mass = 2.4 x 10^4 solar masses.
- speed = 13 km/s.
- radius = 6pc.

Morphology:

- The shell has a well defined eastern arc but it broke open in the west.

Driving force:

- Winds of Wd2 cluster and WR20a is powering the shell.

Previous studies: northern cloud and ridge

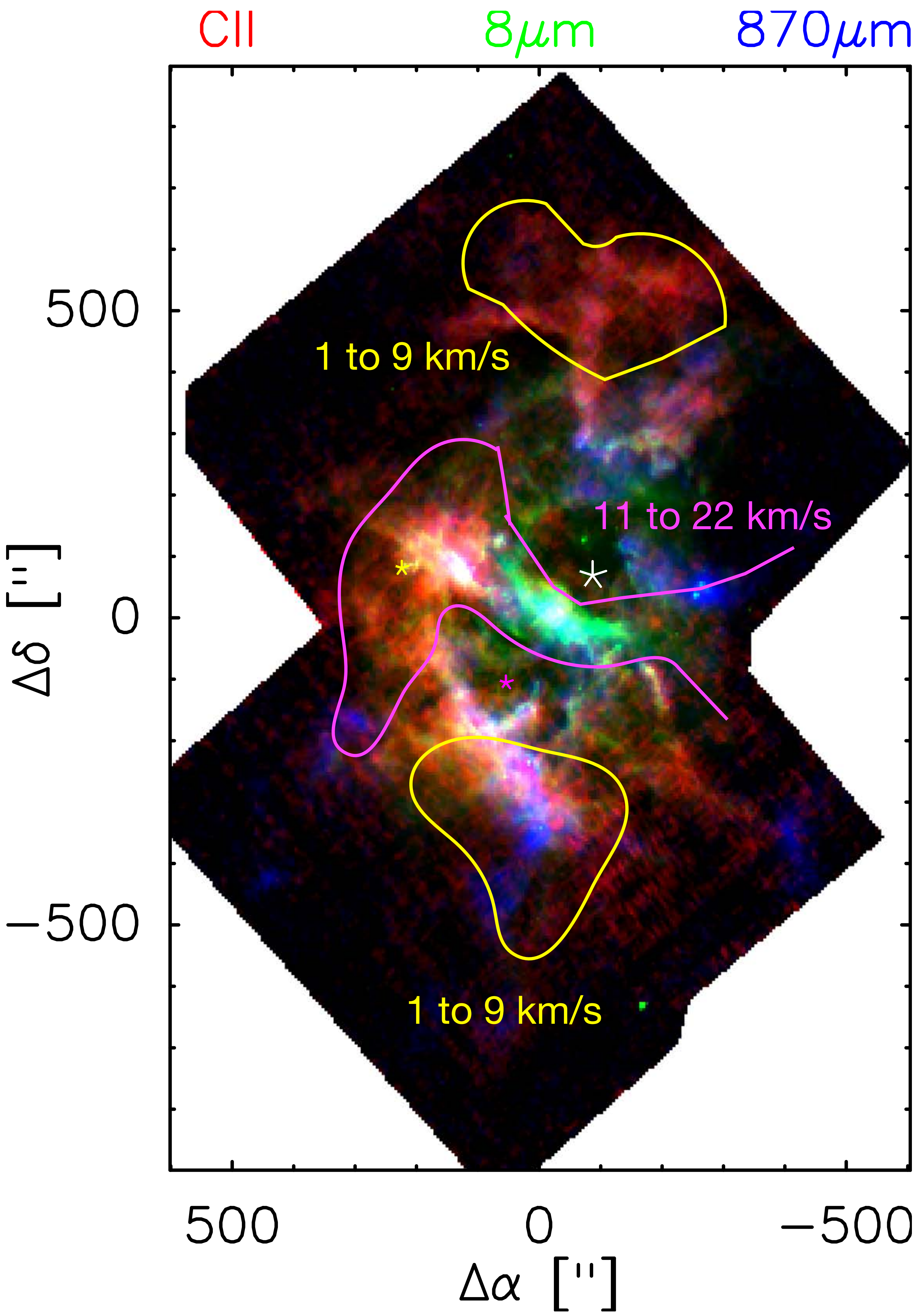

- Furukawa et al., 2009 studied CO 2-1 data.
- Identified two large scale clouds: the northern cloud and the ridge.
- Suggested that their collision led to the formation of Wd2 cluster.

Previous studies: pillar

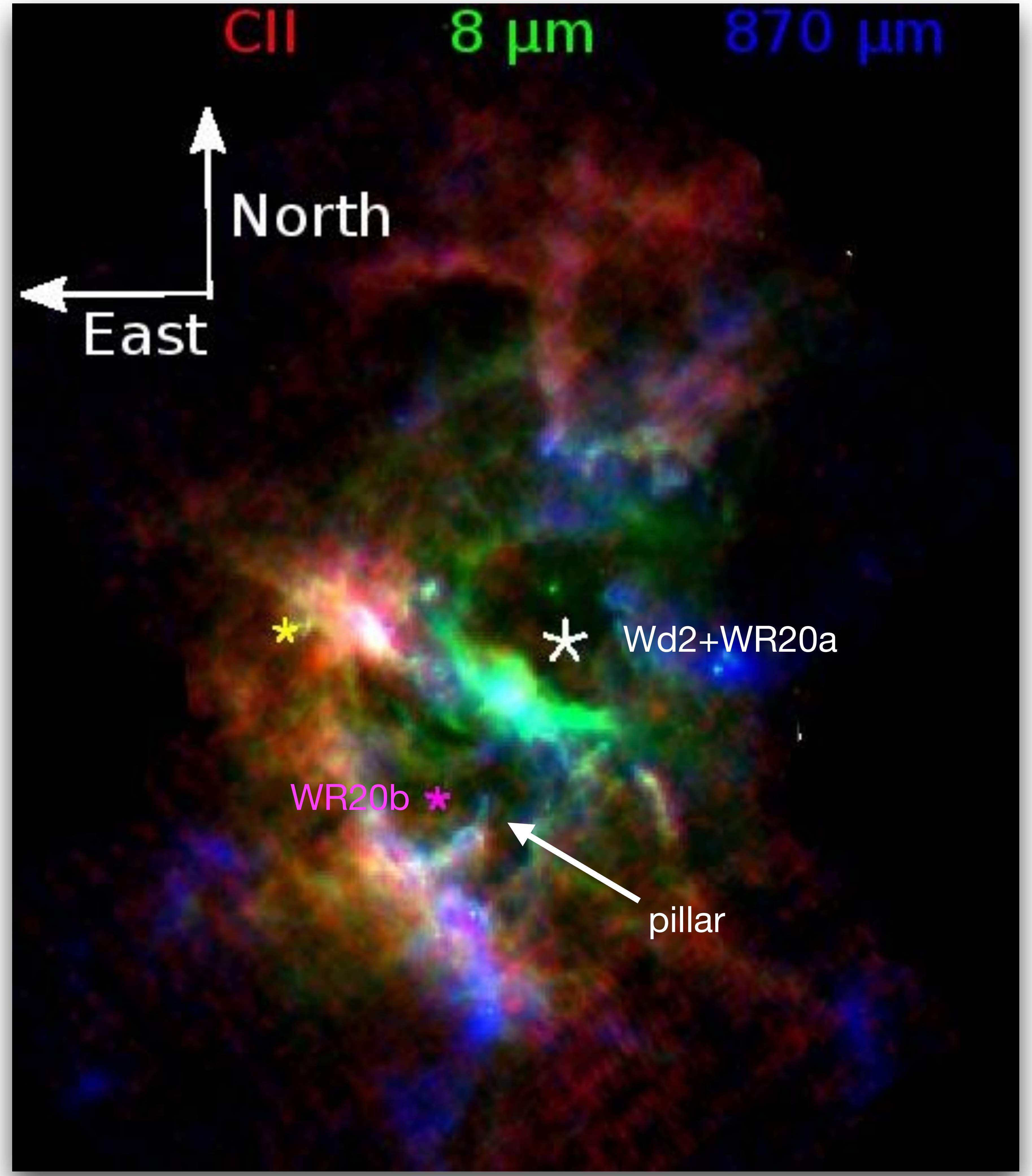

- No independent study has been done on the pillar of RCW49.
- It’s morphology suggests that it is formed from the stellar feedback of Wd2 cluster.
- But WR20b might also affect its physical conditions.

Goals

- Determine the physical conditions in different regions of RCW 49.
- Find the best PDR analysis strategy.
- Understand the impact of stellar feedback in RCW 49.

PDR Analysis

PDR ToolBox (Pound & Wolfire 2008, Kaufman & Wolfire 2006)

Being developed and updated by Mark Wolfire and Marc Pound at UMD.

- It's a tool to determine the physical parameters of photodissociation regions.

- Compared observations with models for different regions of RCW 49.

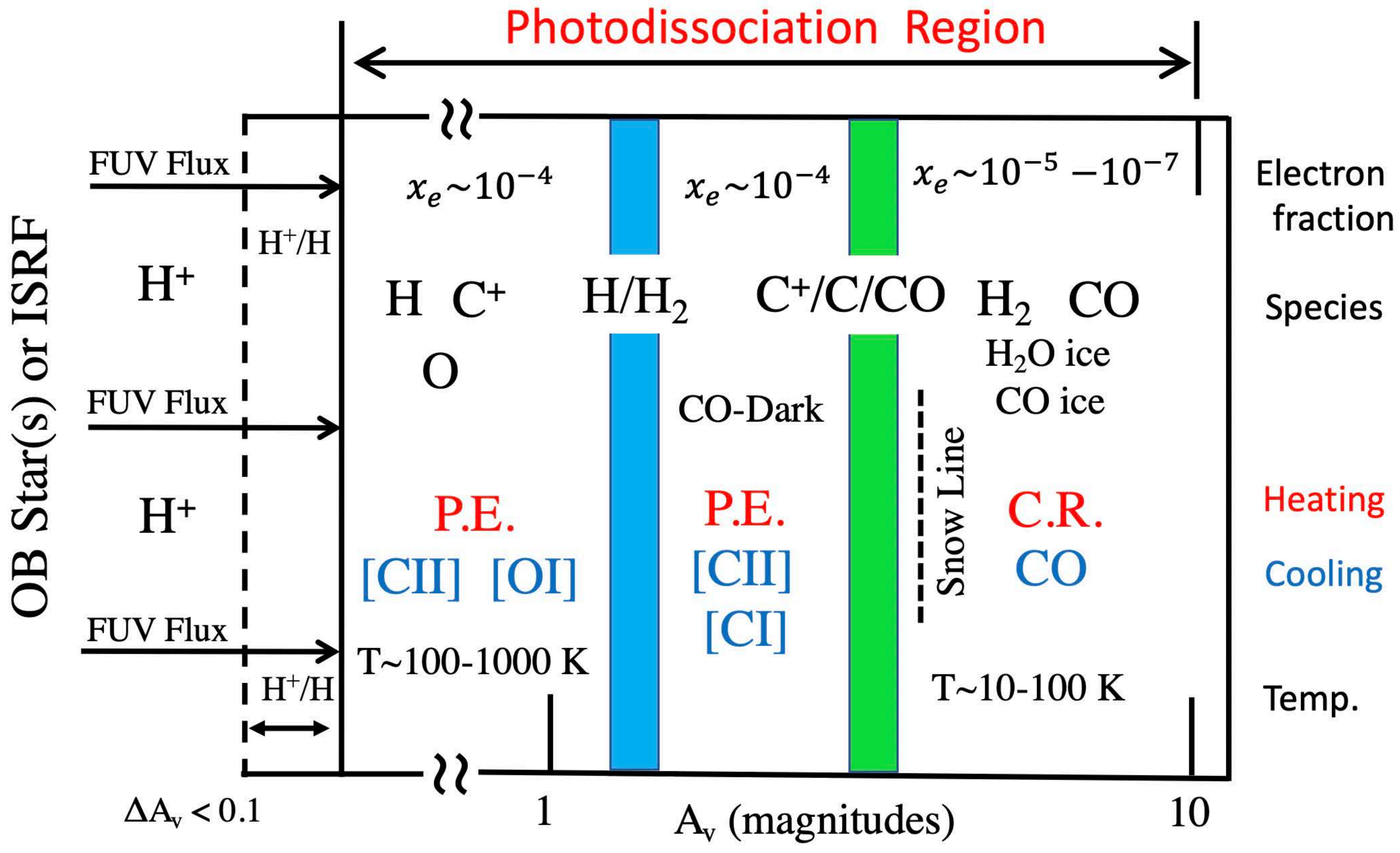

(Wolfire et al., 2022)

Overlay plots

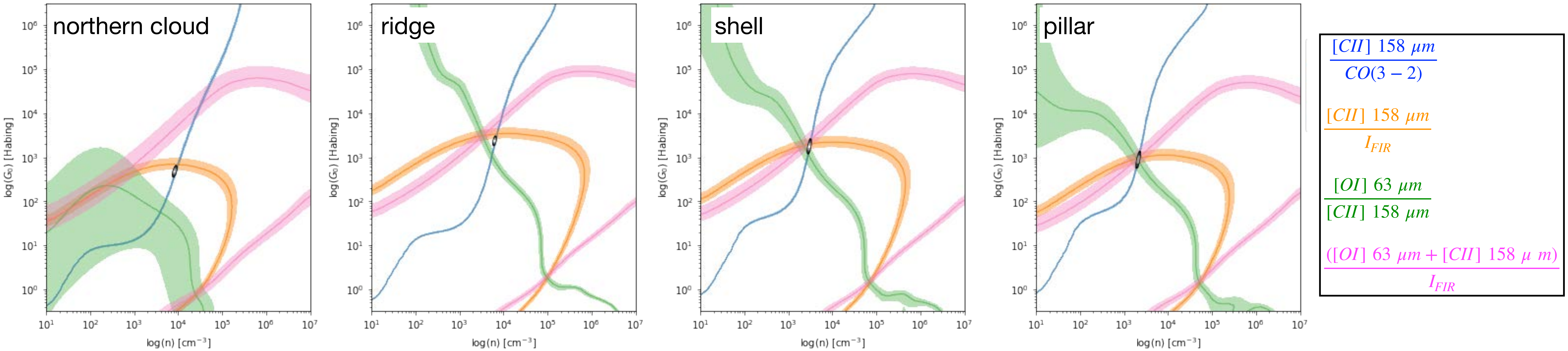

	northern cloud	ridge	shell	pillar
G_0 (Having units)	5.0 x 10^2	2.4 x 10^3	1.9 x 10^3	9.7 x 10^2
$n(cm^{-3})$	8.6 x 10^3	6.4 x 10^3	3.1 x 10^3	2.2 x 10^3

(Tiwari et al. to be sub.)

Phase-space diagrams

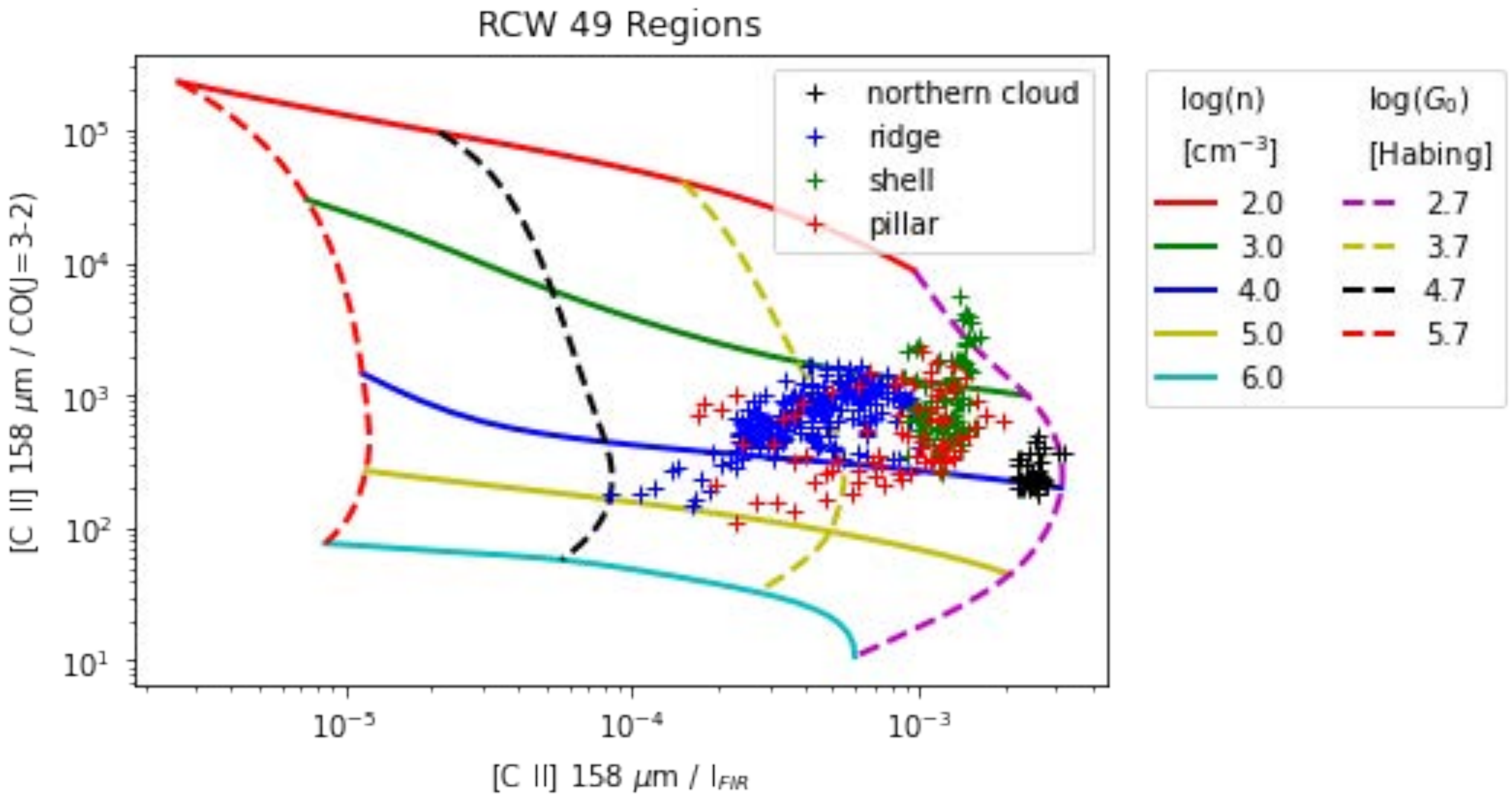

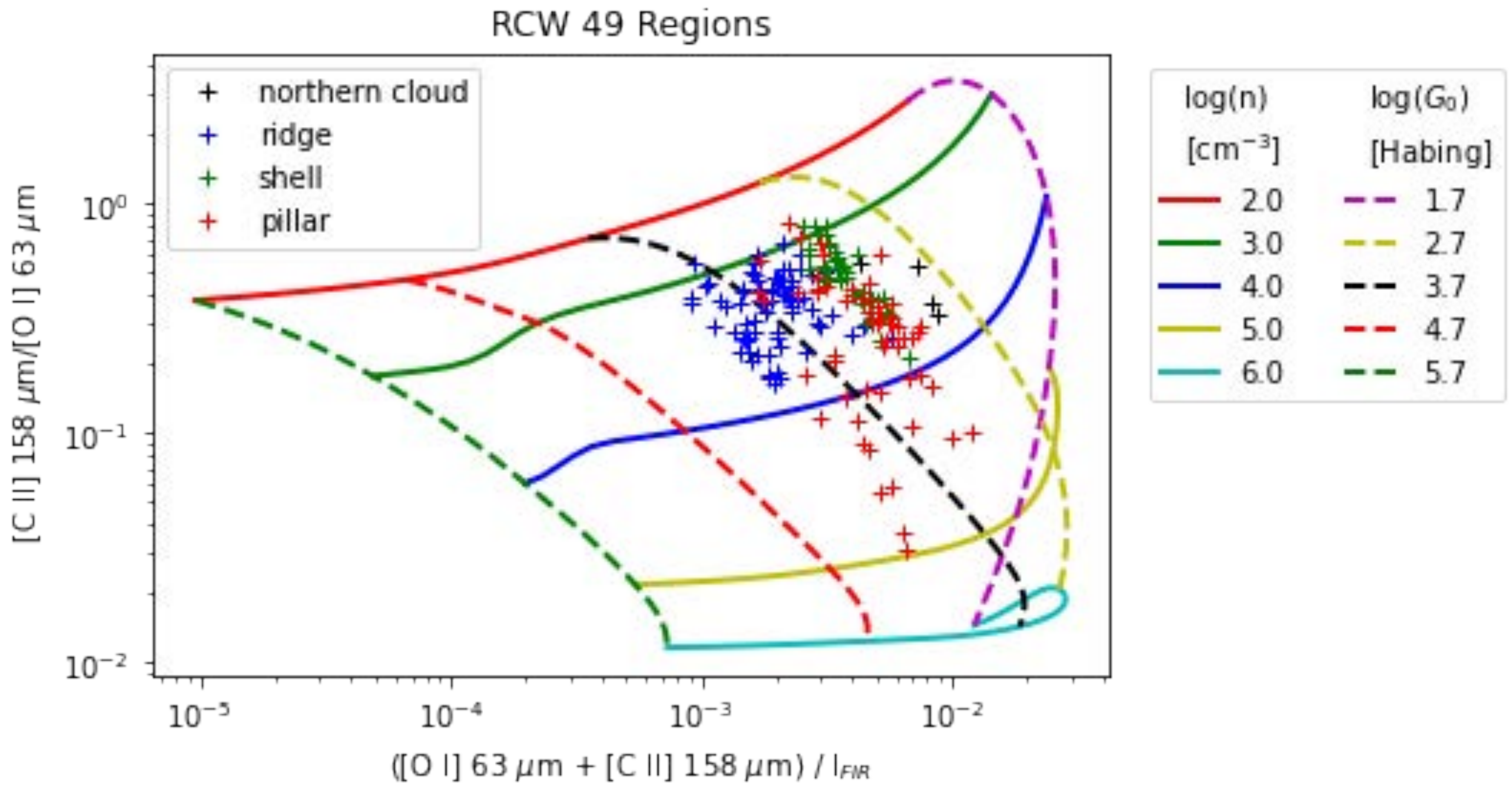

- Overlaying all the data points for every region.
- The spread for the ridge and the pillar is the most.
- Good to visualize the gradients but biased with the choice of ratios.

(Tiwari et al. to be sub.)

Overlay plots vs phase-space diagrams

	Overlay plots	**Phase-space diagrams**
visualize gradient		
number of ratios	4	2
error estimation		

(Tiwari et al. to be sub.)

Overlay plots vs phase-space diagrams

	Overlay plots	**Phase-space diagrams**
visualize gradient	✗	✓
number of ratios	4	2
error estimation	✓	✗

Overlay plots are best at determining physical conditions.

(Tiwari et al. to be sub.)

p_{th} vs G_0

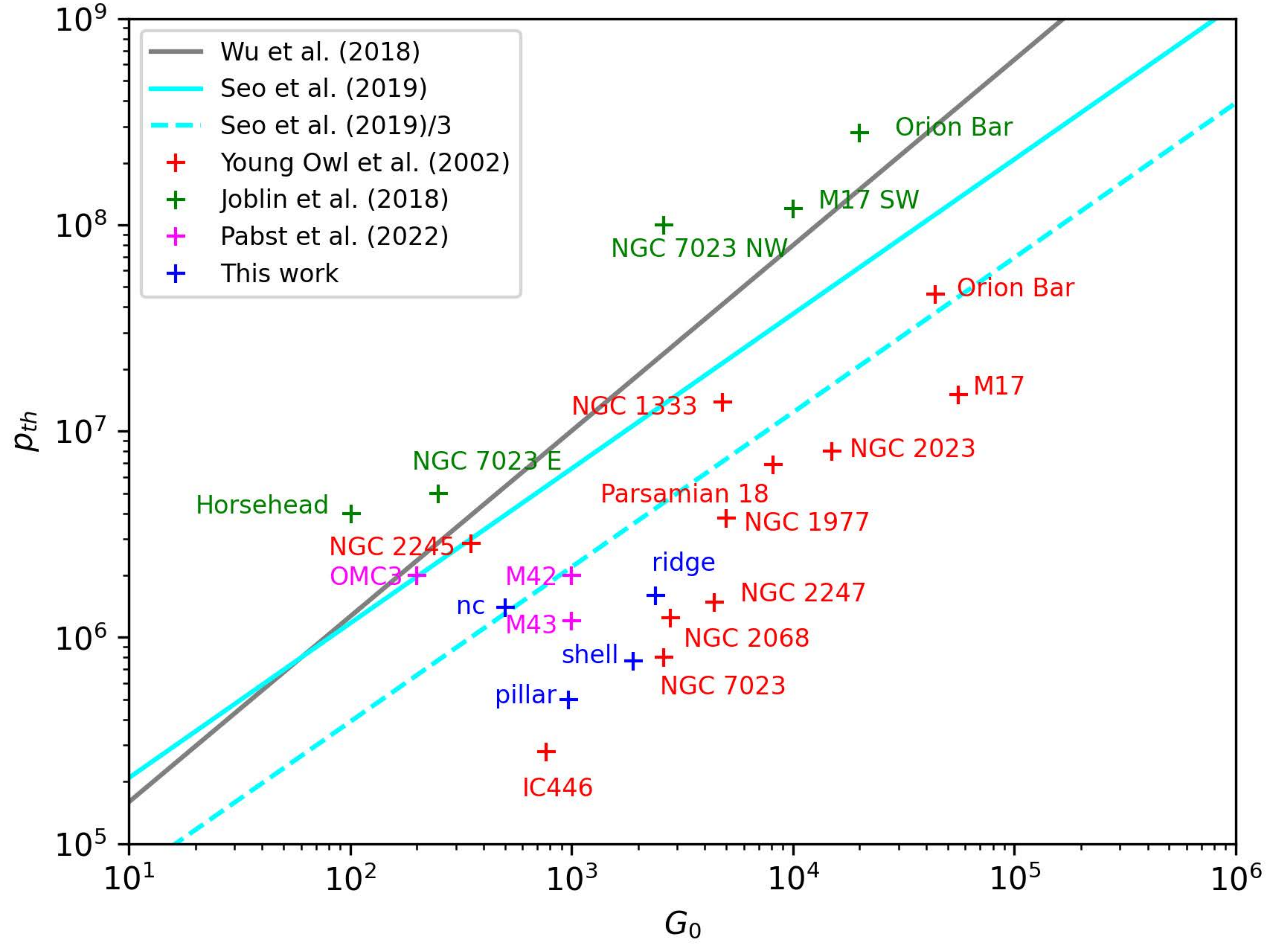

- Young Owl et al., 2002 used FIR lines.
- Joblin et al., 2018 used high-J CO lines.
- Pabst et al., 2021 used low-J CO and [CII].
- Wu et al., 2018 relation based on high-J CO lines.
- Seo et al., 2019 analytical relation for an HII region bordering on a PDR in pressure equilibrium.

Physical conditions in RCW 49 agree well with the basic Strömgren relation.

(Tiwari et al. to be sub.)

Impact of stellar FEEDBACK

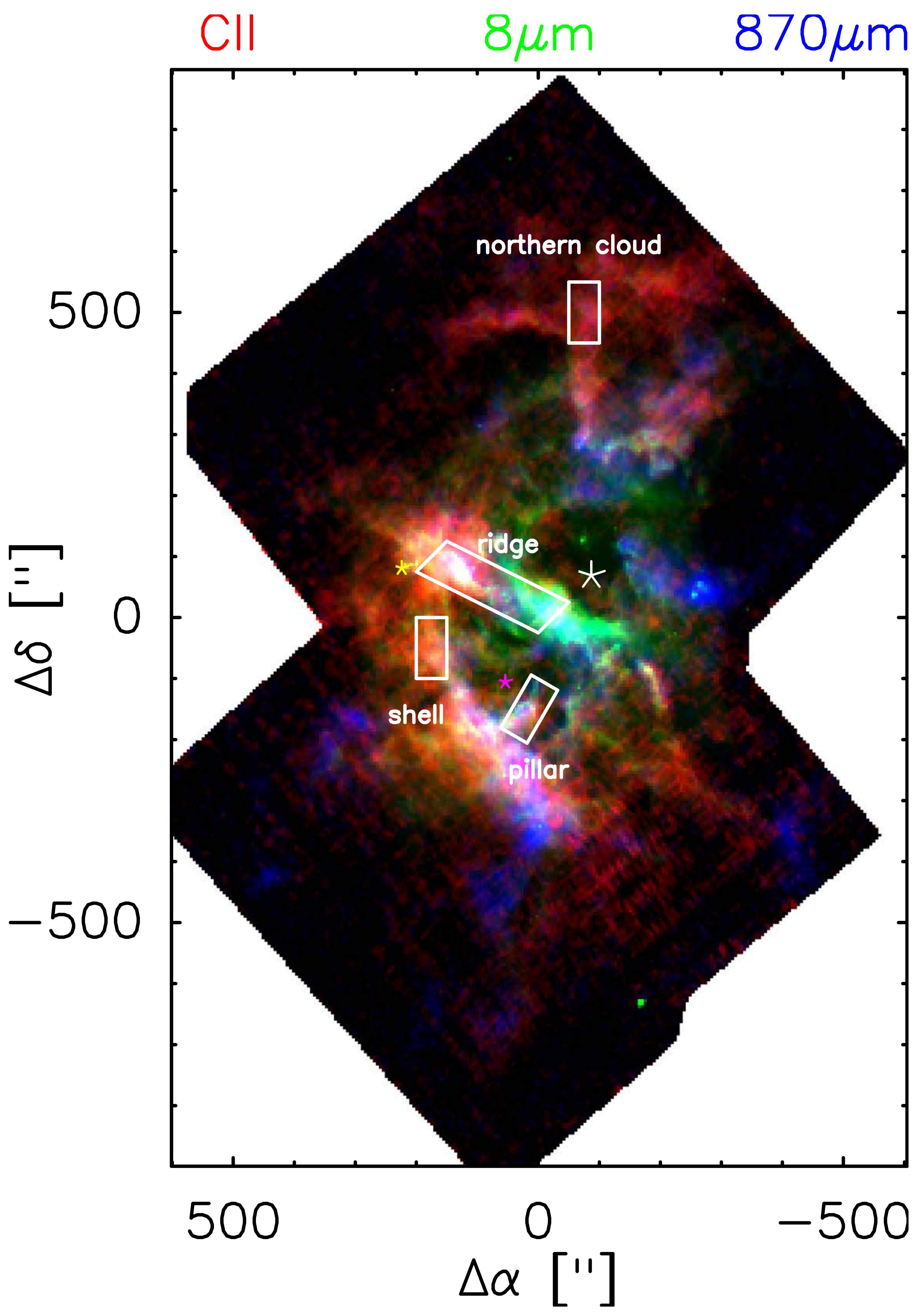

Linking physical conditions to morphology and star formation activity

n: northern cloud > ridge > shell > pillar

- nc and ridge collided to form Wd2 (Furukawa et al. 2009).
- ridge has ongoing vigorous star formation.
- shell has a second generation of star formation taking place with stars lower in mass than Wd2 (Whitney et al., 2004 and Tiwari et al., 2021).

G_0: ridge > shell > pillar > northern cloud

- ridge is the closest to Wd2, nc is > 40 pc away (Furukawa et a. 2009).
- shell is ~ 6 pc away from Wd2 (Tiwari et al., 2021).
- pillar is expected to be at similar distances and powered by Wd2.

(Tiwari et al. to be sub.)

Summary

- Determine the physical conditions in different regions of RCW 49.

- Find the best PDR analysis strategy.

- Understand the impact of stellar feedback in RCW 49.

Summary

- Determine the physical conditions in different regions of RCW 49.
- Northern cloud and ridge have highest n.
- Ridge has the highest G_0 and northern cloud has lowest G_0.

- Find the best PDR analysis strategy.
- Overlay plots are the best to determine physical conditions.

- Understand the impact of stellar feedback in RCW 49.
- We linked the physical conditions with the morphology and star formation activity.

Thank you!

Back up

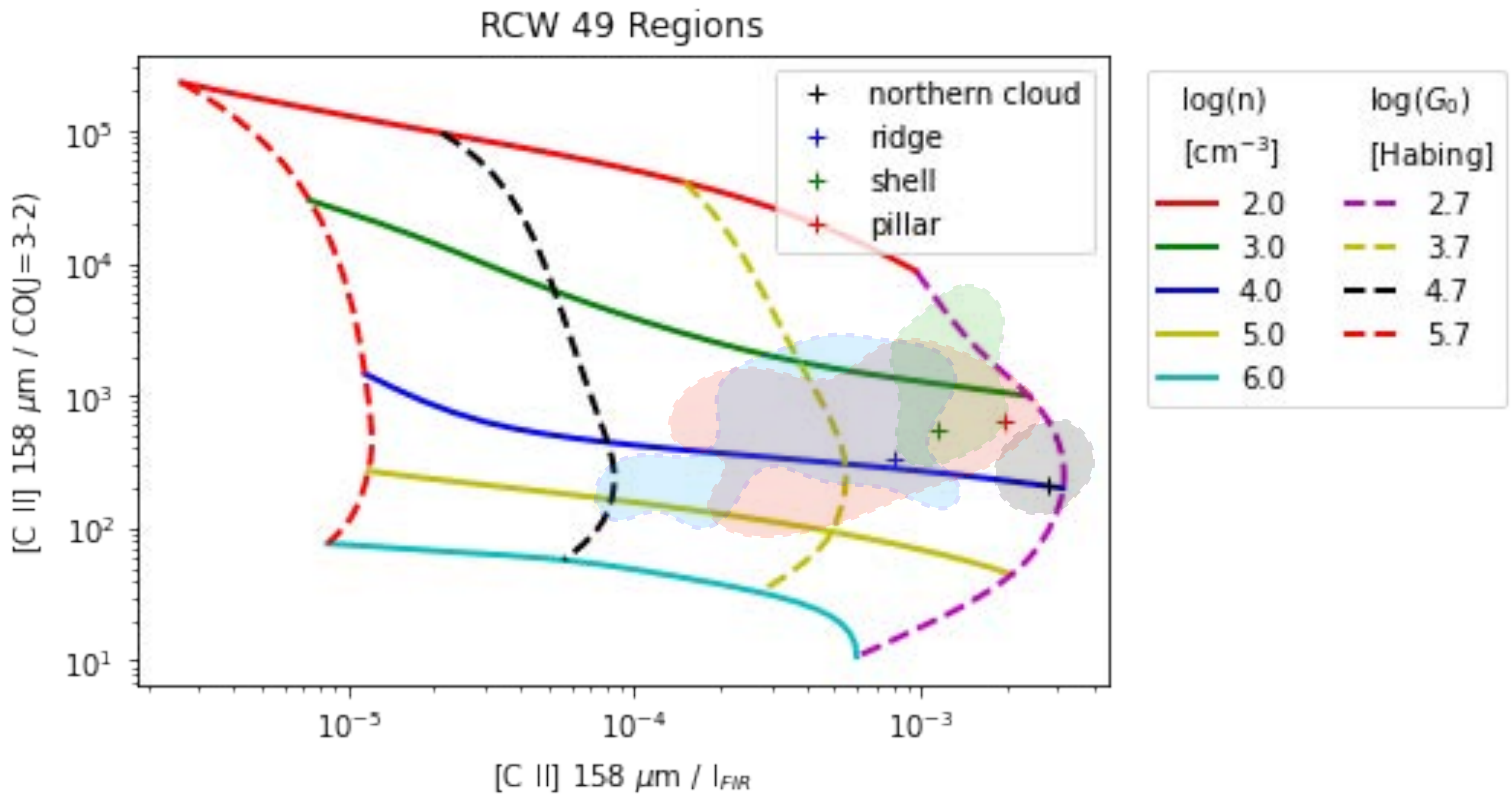

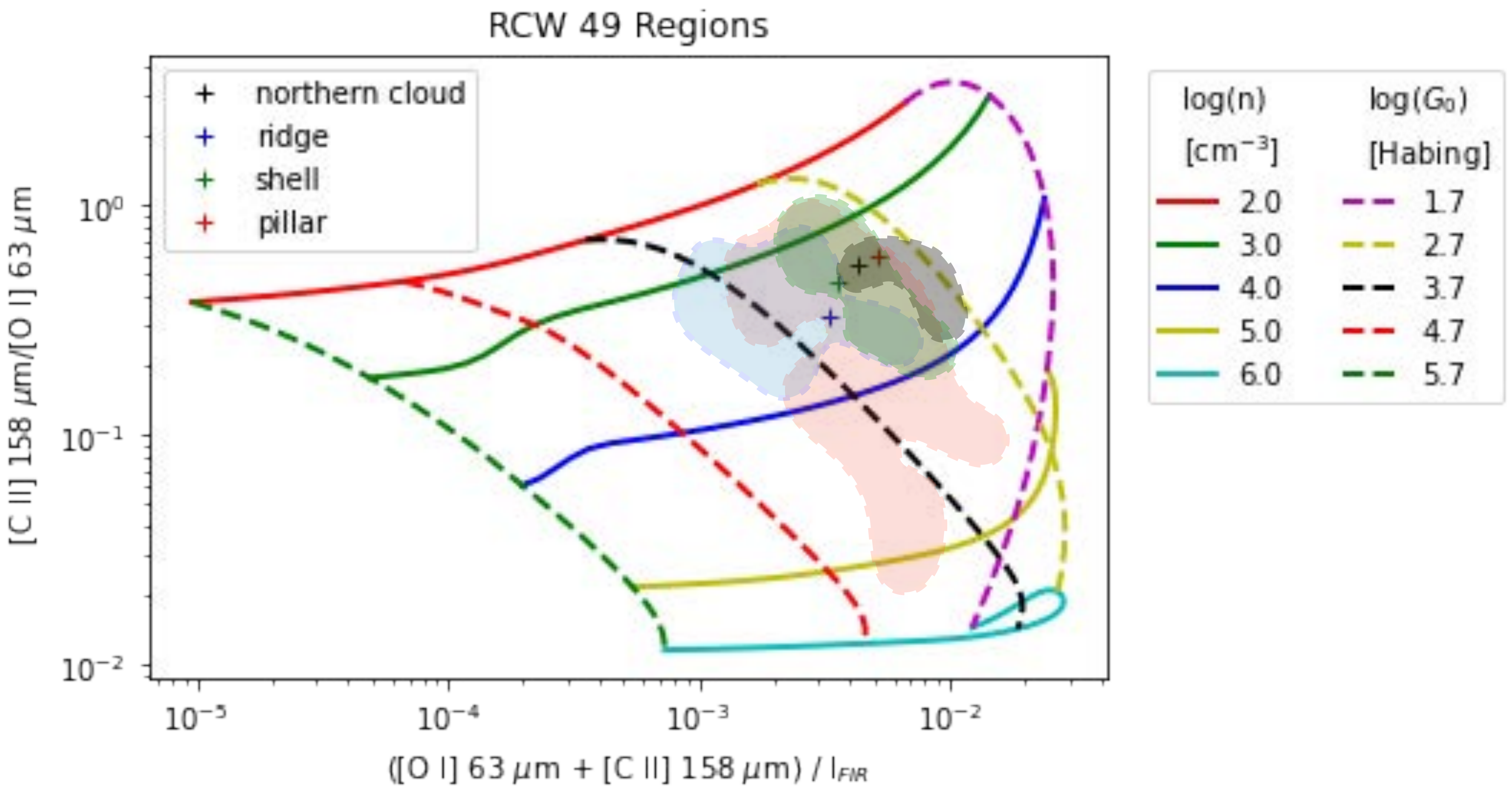

(Tiwari et al. to be sub.)

timescales backup

Stellar wind driven shell with radius = 6pc, velocity = 13km/s, timescale= 0.27 Myr (Weaver et al., 1977)
Age of Wd2 ~ 2-3 Myr, so shell speed can't be > 2km/s

WR20a formed after 2Myrs

Pth-g0 relations backup

pth_seo2=1.233*10**4*(g0**0.75)
pth_wu=2*10**4*(g0**0.9)
pth_seo1=3.7*10**4*(g0**0.75)

backup

Table 2. Derived physical parameters in different regions of RCW 49 .

	northern cloud	ridge	shell	pillar	p1	p3	p7
G_0 (FIR)	9.2×10^2	4.7×10^3	3.2×10^3	2.2×10^3	1.7×10^3	4.8×10^3	1.5×10^3
n (LSQ)	8.5×10^3	6.4×10^3	3.0×10^3	2.1×10^3	2.6×10^4	4.3×10^3 3.6×10^3 4.4×10^3	1.4×10^4
n_{error} (LSQ)	2.9×10^3	9.0×10^2	1.4×10^2	2.0×10^1	2.0×10^4	8.4×10^2 8.6×10^2 1.0×10^3	1.1×10^4
n (MCMC)	8.6×10^3	6.4×10^3	3.1×10^3	2.2×10^3	2.7×10^4	4.3×10^3 3.6×10^3 4.5×10^3	1.4×10^4
n_{error} (MCMC)	4.8×10^2	2.5×10^2	1.5×10^2	1.2×10^2	1.7×10^3	7.9×10^1 7.1×10^1 2.2×10^2	9.1×10^2
G_0 (LSQ)	5.0×10^2	2.4×10^3	1.8×10^3	9.0×10^2	2.8×10^3	2.1×10^3 7.8×10^2 1.9×10^3	3.2×10^4
$G_{0\mathrm{error}}$ (LSQ)	4.4×10^2	1.1×10^3	3.1×10^2	3.2×10^1	3.4×10^3	1.9×10^3 7.1×10^2 1.6×10^3	6.9×10^4
G_0 (MCMC)	5.0×10^2	2.4×10^3	1.9×10^3	9.7×10^2	2.9×10^3	2.1×10^3 7.9×10^2 2.0×10^3	3.2×10^4
$G_{0\mathrm{error}}$ (MCMC)	7.1×10^1	2.8×10^2	3.5×10^2	2.1×10^2	3.2×10^2	1.8×10^2 7.1×10^1 2.2×10^2	7.7×10^3
T_{surface}	160	246	250	223	244	242 196 242	441
p_{th}	1.4×10^6	1.6×10^6	7.7×10^5	5.0×10^5	6.6×10^6	1.0×10^6 7.1×10^5 1.1×10^6	6.2×10^6
p_{turb}	9.4×10^6	3.0×10^6	3.5×10^6	1.8×10^6	2.5×10^7	1.2×10^7 3.9×10^6 1.8×10^6	1.9×10^7

Spectra backup

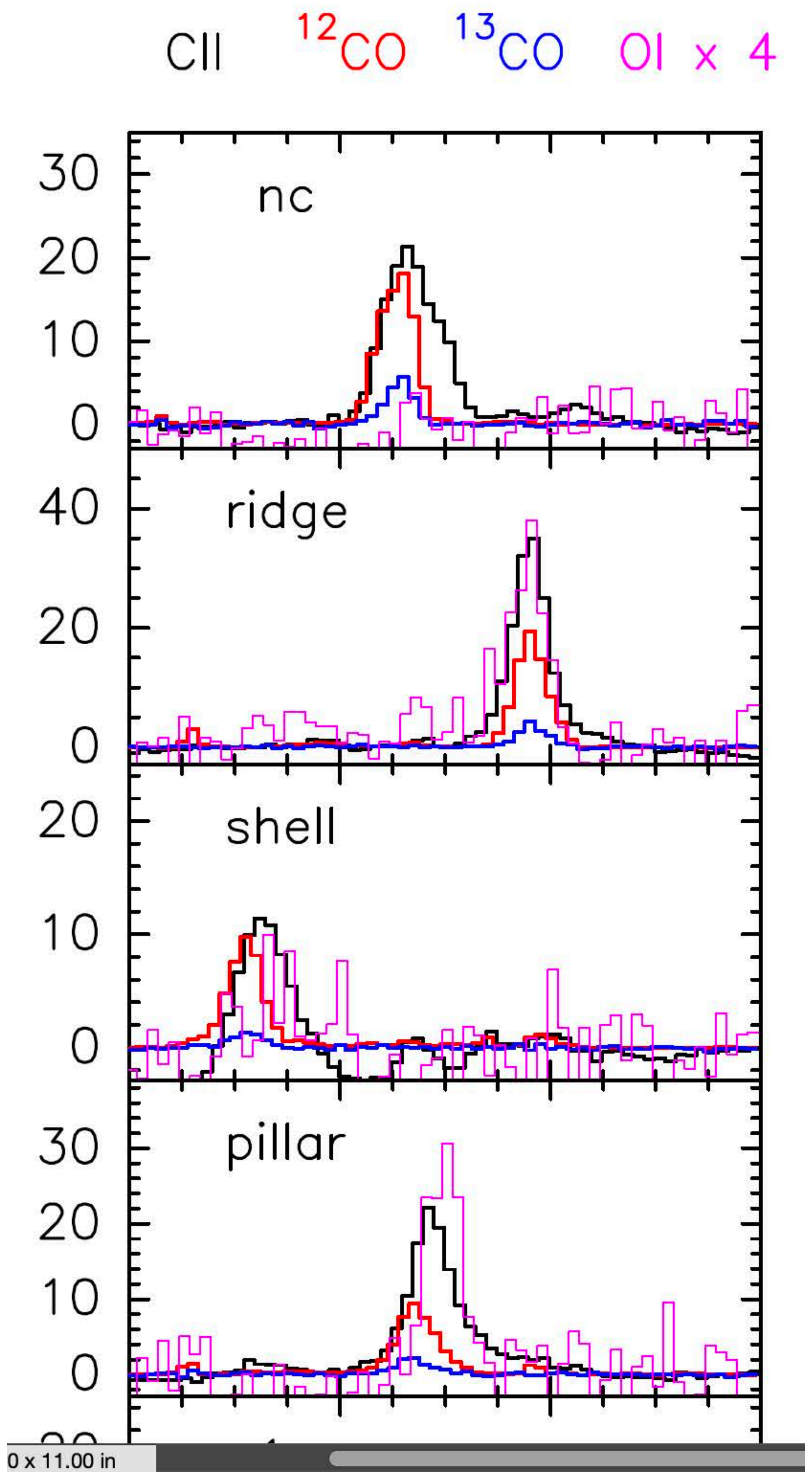

D. OPTICAL DEPTH OF [C II]

We determined the opacity of [C II] emission using its isotope [^{13}C II]. The [^{13}C II] line splits into three hyperfine-structure (hfs) components due to the coupling of angular momentum and spin of the hydrogen nucleus. Due to the limited signal-to-noise (S/N) ratio we have toward any single line-of-sight, we averaged the spectra toward a bright region ($100'' \times 100''$ around $\Delta\alpha = 150''$, $\Delta\delta = 80''$) in [C II], emission, to detect [^{13}C II] lines. We used the $F = 1 \rightarrow 0$ hfs component at 1900.95 GHz, which is the second strongest hfs component with a relative intensity (r_i) of 0.25 (see Guevara et al. 2020, Table. 1), to calculate the total [^{13}C II] intensity. The reason we did not use the brightest hfs component is because it lies within the velocity wing of the [C II] emission, while the second strongest component lies well beyond the velocity range of [C II] emission and can be analysed. The $F = 1 \rightarrow 0$ hfs component of [^{13}C II] is multiplied by the ^{12}C/^{13}C ratio, $\alpha = 52$ (Milam et al. 2005), for a Galactocentric distance of $\sim$ 8 kpc for RCW 49 (using equation 2 of Brand & Blitz 1993).

As can be seen in Fig. 17, we find that the [^{13}C II] spectral emission follows a similar profile as that of [C II] within its higher noise, but the intensity is higher than expected for optically thin [C II], indicative of an optical depth > 1. Using the technique mentioned in Guevara et al. (2020) and using their equation 4, we estimated an optical depth in [C II], of $\tau = 3$. This number should only be taken as a reference because we find that for an rms of 0.8 K, we get a [^{13}C II] peak detection of $\sim$ 1.2 K i.e. a S/N of 1.5. Due to reduced S/N, we were unable to estimate [C II] optical depths toward other regions. So, we take $\tau = 3$ as an upper limit for the entire [C II] emission toward RCW 49.

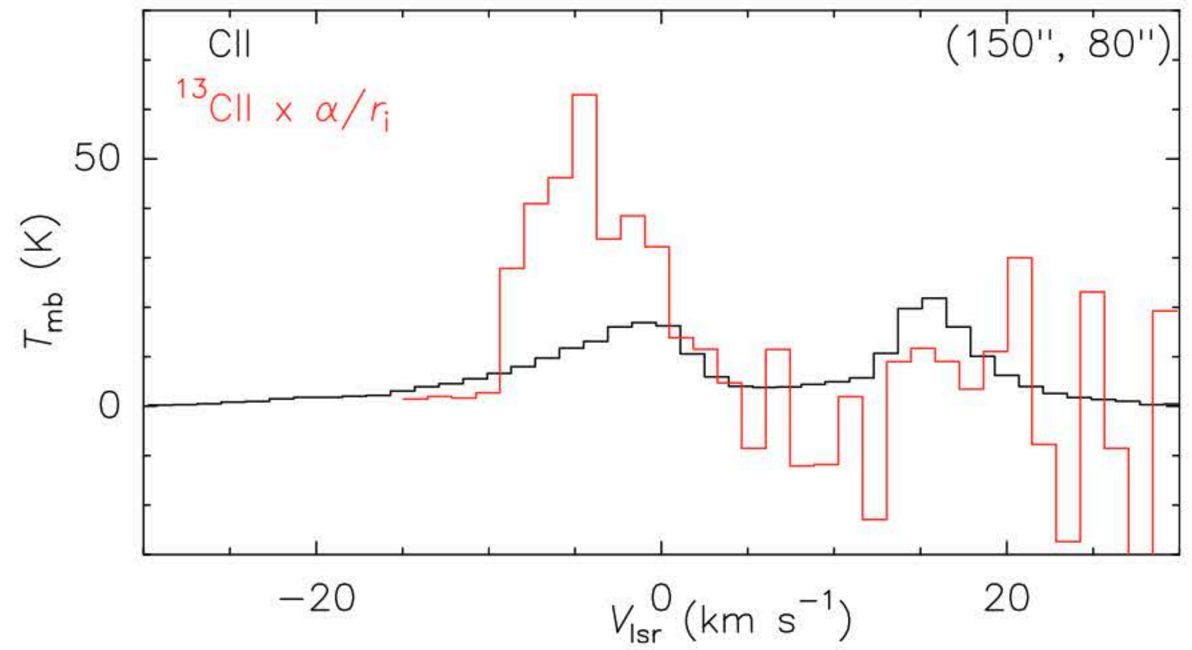

Feedback source sample backup

source	**d(npc)**	**SF activity**	**area(’)**
RCW 36	0.7	O8, B-cluster	15 x 20
RCW 76	4.3	2 O4, 10 late O	20 x 20
RCW 49	4.2	comp. cluster, 2 WR	20 x 30
RCW 120	1.3	O7	15 x 15
NGC 6334	1.3	O8, mini starbust	20 x 35
M17	1.9	2 O4, 10 late O	20 x 30
M16	2	O4, 10 late O	20 x 30
W40	0.26	1 O, 2 B	20 x 30
W43	5.5	mini starbust	15 x 15
Cygnus X	1.4	2 OB, 3 WR, ~50 O	20 x 35
NGC 7538	2.8	O3	15 x 15

Feedback source sample

source	d(npc)	SF activity	area()
RCW 36	0.7	O8, B-cluster	15 x 20
RCW 76	4.3	2 O4, 10 late O	20 x 20
RCW 49	4.2	comp. cluster, 2 WR	20 x 30
RCW 120	1.3	O7	15 x 15
NGC 6334	1.3	O8, mini starbust	20 x 35
M17	1.9	2 O4, 10 late O	20 x 30
M16	2	O4, 10 late O	20 x 30
W40	0.26	1 O, 2 B	20 x 30
W43	5.5	mini starbust	15 x 15
Cygnus X	1.4	2 OB, 3 WR, ~50 O	20 x 35
NGC 7538	2.8	O3	15 x 15